CHALMERS

Development of Structured Illumination Microscopy for Single-cell Studies

Master of Science Thesis in the Master Degree Programme, Biomedical Engineering

CHRISTINA JENSEN
KARIN SÖDERVALL

Department of Signal Processing and Biomedical Engineering
Division of Signals and Systems
CHALMERS UNIVERSITY OF TECHNOLOGY
Gothenburg, Sweden, 2014
Report No. EX005/2014

Development of Structured Illumination Microscopy for Single-cell studies

Christina Jensen
Karin Södervall
Department of Signal and Systems
Chalmers University of Technology

Abstract

There exist different high-resolution imaging techniques when studying single-cell structures and biological matter; modern imaging microscope techniques based on structured illumination (SIM), stimulated emission depletion (STED) or single molecule localization (PALM/STORM). In biological cells, a great number of events take place simultaneously to fulfill all the cell functions and there are a lot of proceeded methods for probing and manipulating the biochemical and physical properties of individual cells. SIM is a non-scanning wide-field technique that can achieve images with a twofold resolution. The advantage of this type of microscopy is the reason that it is easy to implement to a conventional fluorescent microscope and the use of non-expensive lasers and cameras. The purpose of this master thesis is to develop, fabricate and characterize a structured illumination setup on a research laser induced fluorescence/wide-field microscope, and use it for single-cell and nanostructure imaging experiments.
Studies on Human Embryonic Kidney (HEK) 293 and Chinese Hamster Ovarian (CHO) cells were done in order to investigate if the microscopy method could achieve high resolution images. The microscopy method is based that cells are illuminated with a structured grid pattern and three images are acquired at three different grid positions. The results showed that the constructed SIM images from the experiments of the cells resulted in an improved image quality due to the reduction of the out-of-focus fluorescence in the original images. However, the SIM image still contained horizontal lines which should have been eliminated. Further investigations need to be done due to fully eliminate the horizontal lines, for example by optimize fabrication of the grid and improved synchronization in grid positioning and camera.

Keywords: structured illumination microscopy, SIM, high-resolution, grid pattern, grating, fluorescence, piezo control, actuator, optical setup

Abbreviations

SIM	Structured Illumination Microscopy
STED	Stimulated Emission Depletion
SSIM	Saturated Structured Illumination Microscopy
LNT(s)	Lipid Nanotube(s)
TRP	Transient Receptor Potential
TRPV1	Transient Receptor Potential Vanilloid 1
NA	Numerical Aperture
PSF	Point Spread Function
FWHM	Full Width at Half Maximum
UV	Ultraviolet
TIRF	Total Internal Reflection Fluorescence
CCD	Charge-Coupled Device
SLM	Spatial Light Modulator
PALM	Photo-Activated Localization Microscopy
STORM	Stochastic Optical Reconstruction Microscopy
STM	Scanning Tunneling Microscope
AFM	Atomic Force Microscope
PCA	Piezoelectric Ceramic Actuator
PDA	Piezoelectric Driver Amplifier
HEK 293	Human Embryonic Kidney 293
CHO	Chinese Hamster Ovarian
MEM	Minimum Essential Medium
ECB	ExtraCellular Buffer
HEPES	*4-(2-hydroxyethyl)-1-piperazineethanesulfonicacid*
FBS	Fetal Bovine Serum
FM1-43	*N*-(3-Triethylammoniumpropyl)-4-(4-(Dibutylamino) Styryl Pyridinium Dibromide
OD	Optical Density
CW	Continuous Wave

Table of Contents

1 Introduction

The magnification in optics is the enlarged view of an object by the use of optical instruments that cannot be magnified by the naked eye. Cells and vesicles are within of the range of hundreds of nanometers to microns; therefore it requires a microscope for the human eye to visualize and manipulate it (Stepanyants, 2013). Observing objects in a microscope can either be done by eyes, cameras or other preferable detectors. However, dependent on that the optical resolution of light microscopy is limited to approximately half of the wavelength of the light used, it can only resolve cellular structures and objects that are at least 200 to 350 nm apart, even with optimal alignment and perfect lenses. Microscopy methods can vary from simple setups, such as standard bright-field microscopes, to more complex ones, such as fluorescence microscopy including confocal microscopy.

There are different imaging techniques when studying single-cell structures and biological matter; modern imaging microscope techniques based on structured illumination (SIM), stimulated emission depletion (STED) or single molecule localization (PALM/STORM). Since recent years several super-resolution fluorescence microscopy methods can achieve extreme high resolution and the nanostructures of cells can therefore be studied with proper imaging technique. In biological cells, a great number of events take place simultaneously to fulfill all the cell functions and there are a lot of proceeded methods for probing and manipulating the biochemical and physical properties of individual cells (Ainla et al., 2010).

Microscope techniques for high-resolution images are expensive and the lack of a relatively cheap modern imaging technique that can image fast movements of cells with high resolution, limits some applications of research concerning nanostructures.

Structured illumination microscopy is a non-scanning wide-field technique that can achieve images with improved resolution. The advantage of this type of microscopy is that it is easy to implement to a conventional fluorescent microscope, the use of non-expensive lasers and conventional CCD cameras and less raw image data to acquire. The disadvantage of SIM is that the process of acquiring images makes this method somewhat slow and when observing the sample, artifacts can appear if the sample is moving during the acquisition. Artifacts such as blurring in the modulated images can therefore be observed (Chasles et al., 2007).

The purpose of this master thesis is to develop, fabricate and characterize a structured illumination setup on a research laser induced fluorescence/wide-field microscope, and use it for single-cell and nanostructure imaging experiments.

The thesis is organized as follows. In Section 2, the interest of single-cell analysis and nanostructure imaging will be presented. Fundamentals of microscopy and the piezoelectric effect will subsequently be introduced. The methodology and materials will be discussed in Section 3, followed by Section 4 wherein the results will be presented. Finally, a discussion and a conclusion will be presented in Section 5 and Section 6, respectively.

2 Background

Microscopy has been the main key in cell biology from the very beginning since the first studies of biological structures in the 17th century. Even though improved image quality has been achieved by manufacturing and technical development, the optical resolution is still a challenging combat. Optical microscopy has become one of the most powerful diagnostic tools in modern cell biology along major innovations including fluorescence and confocal laser scanning microscopy (Schermelleh, 2010). The development of fluorescence microscopy has been central in order to understand and elucidate cellular functions beyond the resolution limit (Kohl et al., 2012).

2.1 Life science studies

Single-cell analysis reveals localized and specified biological information of individual cells. Local environmental control techniques, i.e. techniques changing and sensing the environment around single-cells, are desired when analyzing the properties of single-cells (Nogawa et al., 2007). Compared to traditional bioanalytical or biotechnological approaches, single-cell studies may contribute to more significant advantages since cellular and subcellular processes can be observed in greater details (Ainla et al., 2010).

2.1.1 Single-cells and lipid nanotubes

Life-maintaining molecular activities such as transport, sensing, biochemical synthesis and information processing are complex nanoscale infrastructures developed by biological cells. Structures common in such biological systems, in order to *e.g.* establishing cell-to-cell connections, are nanotubular structures. Vesicle-nanotube networks are soft-matter constructions in the micro- and nanoscale size that can serve as models for interlinked biochemical reactors and in order to create, investigate and apply these networks for chemical reactions and transport, a variety of microscopy setups has to be integrated with prominent methods (Jesorka et al., 2011).

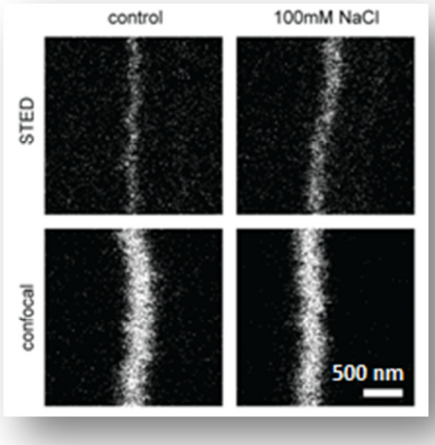

Figure 1 Nanotube diameter measurements with STED microscopy (Stepanyants et al., 2013)

Essential elements in all living cells are lipid membranes, where the mechanical properties of these membranes can be modified by compositional changes and binding of solutes. These modifications can be monitored through the size of extracted nanotubes. The tracking of radii

response to various stimuli is enabled by a membrane displacement lipid nanotube sizing technique that results in a measurement of the membrane bending rigidity (Stepanyants et al., 2013). In Figure 1, one can see the diameter change of a nanotube imaged with super-resolution technique (STED) and confocal microscopy when having 0 (control) and 100 mM NaCL present. The change in the diameter of the nanotube is more distinguished in the STED image compared to the confocal image, and therefore STED microscopy is well-suited for this kind of applications (Stepanyants et al, 2012).

2.1.2 Ion channel

In Figure 2, a basic structure of an ion channel is shown. Ion channels are an important part of the cell membrane and they exist as pore forming proteins. An ionic concentration difference is maintained by an active barrier; the plasma membrane, such that the intra and extra cellular environment is separated. Hormonal secretion, blood pressure regulation, learning and memory are processes where ion channels are crucial and they exist in the membranes of all plant, bacterial and plant cells. A number of both animal and human diseases are related with the function of the ion channels when they not work properly. Ion channels open and close upon what kind of stimuli that occurs and the ion channels are classified dependent on what stimuli they react on. They can either be voltage gated channels, ligand gated channels or physiological (mechanical, temperature) stimulus channels (Ahemaiti, 2010).

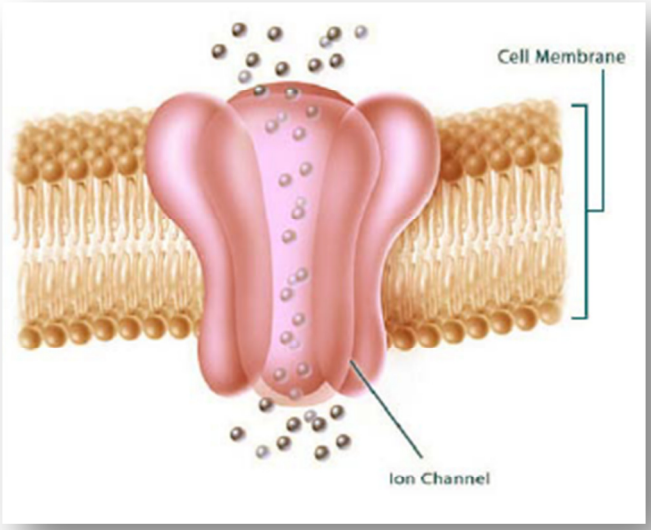

Figure 2 Ion channel structure (Ahemaiti, 2010)

Ion channels reacting on temperature or mechanical change are either inactivated or activated by mechanical stress. Our sensory system is guarded by transient receptor potential (TRP) ion channels, which react on temperature, pain, taste, touch or other similar stimuli. Depending on what stimuli the TRP ion channels react on, they can be divided into seven subgroups consisting of TRPV, TRPC, TRPM, TRPN, TRPA, TRPP and TRPML. TRPV is for example ion channels responding to heat and TRPAs are sensors responding to cooling. Each of all the groups have six transmembrane domains, where *e.g.* TRPV1 (transient receptor potential

vanilloid 1) ion channel is activated when the temperature reaches 42º or 43º and they are found in the peripheral nervous system, spinal cord, tongue, bladder and brain. Protons, voltage and ligands can also activate TRPV1 ion channels, *e.g.* a strong activator of TRPV1 is the main vanilloid compound in chili; Capsaicin. This explains why one can sometimes feel heat pain when eating chili (Ahemaiti, 2010).

2.2 Microscopy fundamentals

Cells and vesicles are within of the range of hundreds of nanometers to microns; therefore it requires a microscope for the human eye to visualize and manipulate (Stepanyants, 2013). The optical resolution of light microscopy is limited to approximately half of the wavelength of the light used, even with optimal alignment and perfect lenses. With this limitation of resolution, the light microscopy can only resolve cellular structures and objects that are at least 200 to 350 nm apart. As mentioned in section 2.1, much of the fundamental biology of the cell occurs at the size range of tens to few hundred nm (Schermelleh, 2010). One attractive optical technique capable of generating high-resolution images of tissue microstructures is fluorescence microscopy (Fu et al., 2013).

2.2.1 Objective lens and numerical aperture

The most important piece of any light microscope is the objective lens that is characterized by several parameters. Among them, the parameters of interest when choosing proper objectives for desired image formation are the magnification and numerical aperture (NA). The definition of magnification in optics is the enlarged view of an object by the use of optical instruments that cannot be magnified by the naked eye. The magnification is typically illustrated on the objective lens by a number that corresponds to the desired size of magnification followed by X, *e.g.* 10X, 20X, 40X and 60X. Numerical aperture is defined by $NA = n \sin \alpha$, where n is the refractive index of the embedding medium and α is the half-angle of the objective's collection cone, which is illustrated in Figure 3. The amount of light that is collected by the objective is roughly said to correspond to the size of the NA since the larger cone of collection light, α, the more light will be collected by the objective, *i.e.* a large NA collects more light compared to a low-NA lens (Piston, 1998).

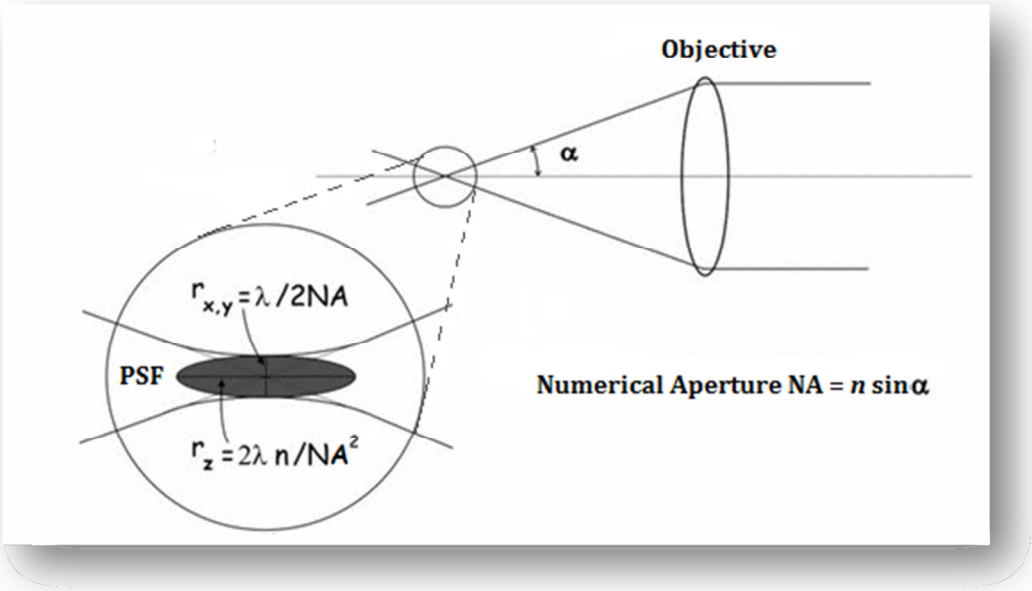

Figure 3 Concept of the objective, NA and PSF (Quercioli, 2011)

Depending on size of sample that will be studied, the highest possible magnification is not necessarily the best solution, since the maximal magnification is limited by the resolution of the optical instruments. The smallest distance of where two objects can be distinguished and discerned as two objects is the definition of resolution. There exist many mathematical definitions of resolution, however, the Abbe diffraction limit is probably the most simple and reasonable quantity, expressed by $R = \frac{\lambda}{2NA}$, where the wavelength of light is denoted by λ. Using this relationship, several experimental values indicate that the smallest resolvable distance is ~200 nm, done by using a large NA lens and laser wavelength λ=500 nm.

The image resolution needs to be matched with the pixels on the detectors when images are detected by detectors instead of eyes. The Nyquist criterion should be considered when calculating the optimal magnification in order to maximize the information content in images, meaning that two points per resolution size should be collected, *i.e.* the sampling rate should be twice the resolution (Piston, 1998).

2.2.2 Point spread function

The point spread function (PSF) depends on the optical properties of the microscope objective, mainly the NA, and the wavelength of light (λ). The PSF, see Figure 3 above, can be described as a point-like object that is spread out in the image where the shape of the PSF can determine the level of detail that can be distinguished in an image and the quality of the imaging system. The smaller PSF, the smaller distance distinguishing two objects from one another and vice versa (Schermelleh, 2010). The full width at half maximum, FWHM, typically describes the shape of the PSF and it expands hundreds of nanometers laterally, expressed by $FWHM \approx \frac{\lambda}{2NA}$, and axially, expressed by $FWHM \approx \frac{2n\lambda}{NA^2}$ (Quercioli, 2011).

2.2.3 Fluorescence microscopy

The result of fluorescence is when inorganic or organic specimens absorb and emit light. Stokes coined the term “fluorescence” when he illuminated ultraviolet (UV) light at the

mineral fluorspar in the middle of the 19th century. He observed that the mineral emitted red light when illuminated with UV, and he also noted that fluorescence emission occurred at longer wavelengths compared to the excitation light (Spring, 2003).

Some specimens autofluoresce when irradiated. However, when the autofluorescence is faint or nonspecific, *e.g*. pathogens or study of animal tissues, fluorochromes (fluorophores) or dyes are added to the specimen. Fluorophores are stains that emit light of useful intensity when excited by a specific irradiating light wavelength and they have the ability to attach themselves to structures that are visible or subvisible organic matter. The development of fluorophores with excitation and emission with known curves of the intensity is well linked with the growing use of fluorescent microscopes. A drawback of fluorescence microscopy is the tendency of photo-bleaching which appear when the fluorescent molecules interact with molecular oxygen in the excited state (Spring, 2003).

The concept of the fluorescence microscope is to illuminate a specimen with light at the excitation wavelength of a fluorophore, while separating and collecting the weaker fluorescent (emitted) light from the excitation light. The eyes or other detectors, *e.g.* camera, are parts wherein the emitted light will reach, resulting in areas of fluorescence contrasted against a dark background, where the darkness of the background mostly determines the detection limit (Spring, 2003). The entire field of view is illuminated uniformly with the excitation light in the conventional fluorescence microscopy, where fluorophores outside the plane of focus also excite and emit photons resulting in a large amount of unwanted background fluorescence. This causes a reduction of the contrast in the region of interest in the focal plane, which is a common problem in wide-field fluorescence microscopy (Fu et al., 2013).

Microscopy techniques rejecting background fluorescence are techniques capable of optical sectioning, which means removal of the contributed out-of-focus light in each image plane from the acquired images of thin slices of a thick sample. Confocal microscopy, total internal reflection fluorescence microscopy (TIRF), wide-field illumination and spinning (Nipkow) disk confocal microscopy are examples of microscopy techniques capable of optical sectioning. The concept of all confocal microscopes is to scanning the illumination through individual areas in sequence simultaneously as scanning the detection (Conchello & Lichtman, 2005). Another approach rejecting background fluorescence is structured illumination microscopy, where a structured illumination light is applied to the conventional fluorescence microscopy, which will be further discussed in Section 2.3.

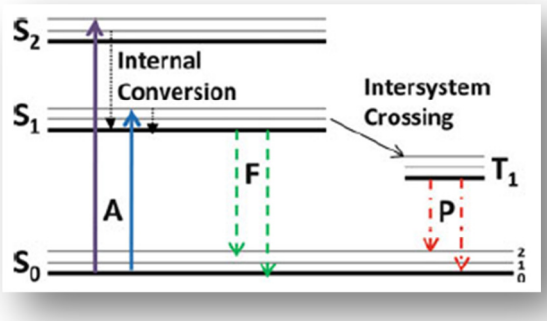

Figure 4 Fluorescence described by Jablonski diagram (Sun & Periasamy, 2013)

The process of fluorescence can be illustrated by a Jablonski diagram, see Figure 4. The singlet ground represents S_0 and the first and second electronic states are represented by S_1 and S_2. The fluorophores can exist in three different vibrational energy levels at S_0, S_1 and S_2. Illustrated above, a light absorption of a solid excites a fluorophore to a higher vibrational level at the electronic states, indicated by the purple and blue arrow. The excited molecule will quickly relax to the lowest vibrational level of S_1 by an internal conversion process. The fluorescence emission (green dotted arrow) typically results from this relaxation of the molecule and then the molecule returns to the ground state S_0 and reaches thermal equilibrium. The energy of the absorbed photon is thus typically higher than the energy for the emitted photon, where the excess of the excitation energy is converted into thermal energy. The first triplet state is denoted by T_1 where the emission is called phosphorescence (red dotted arrow) instead of fluorescence. Compared to S_1, T_1 is a long lived state which has a smaller energy gap between T_1 and S_0 and therefore are longer wavelengths relative to fluorescence emitted (Sun & Periasamy, 2013).

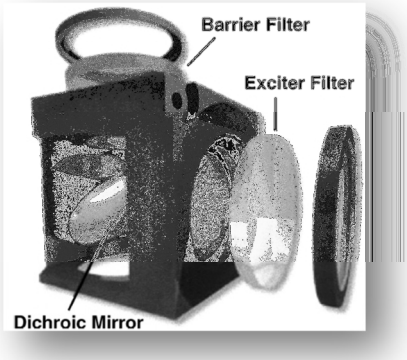

Figure 5 A filtering system containing barrier and exciter filters with a dichroic mirror assembled as a cube (Spring, 2003)

Inside the fluorescence microscope, two parts are playing the key role; the objective and a filtering system called beam splitter. This beam splitter contains a dichroic mirror, barrier (emission) filter and an exciter (excitation) filter, often assembled in a structure of a cube. As can be seen in Figure 5, the dichroic mirror is placed at a 45° angle in the cube between the filters, facing the excitation light path in order to be reflective and transmissive at certain

wavelengths. The principle of the cube assembly is to direct the selected excitation light through the objective and then onto the specimen, and directing longer wavelengths to the barrier filter and scattered excitation light is reflected back to a part of the microscope called the lamphouse (Spring, 2003).

2.3 Structured illumination microscopy

There are since recent years several fluorescence microscopy methods for single-cell studies that can achieve high resolution. These can roughly be divided into either as a near-field or a far-field microscopy approaches. The difference between them is that near-field microscopy is easy to implement in fields of cell biology when imaging surface structures and dynamics, while far-field microscopy can be used to image the interior of the cell. A major near-field microscopy approach in cell biology is the use of total internal reflection fluorescence (TIRF) (Schermelleh et al., 2010). However, this microscopy method will not be described further in this study.

There are three prominent applicable far-field methods in fluorescence microscopy that will be discussed in this section; structured illumination microscopy (SIM), stimulated emission depletion (STED) and single molecule localization (PALM/STORM) (Schermelleh et al., 2010).

2.3.1 Fundamentals of SIM

Structured illumination microscopy is, as mentioned above, a far-field fluorescence microscopy approach, which is linear and can two-fold the resolution (Kner et al., 2009). It is categorized as a wide-field method since it is based on acquisition of a set of individual images at different positions of an illumination mask, with a defined pattern, at a given focus plane without any mask in the detection beam path. This approach can for example be illustrated as in Figure 6 (Heintzmann, 2006).

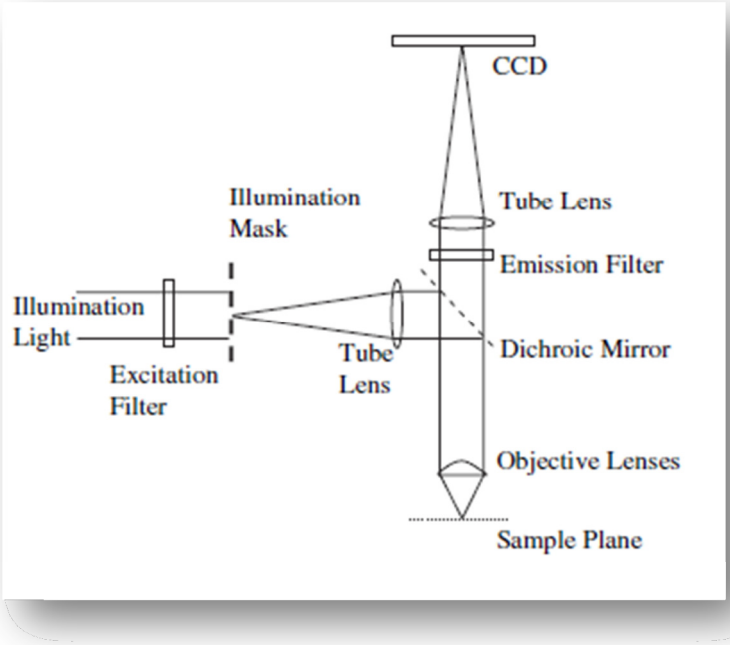

Figure 6 Example of a basic experimental setup to acquire data from structured illumination (Heintzmann, 2006)

The principle of SIM (Neil et al., 1997) is to illuminate a sample with a single-spatial-frequency grid pattern, see Figure 7, and the microscope will consequently display only that part of the sample where the grid pattern is in focus.

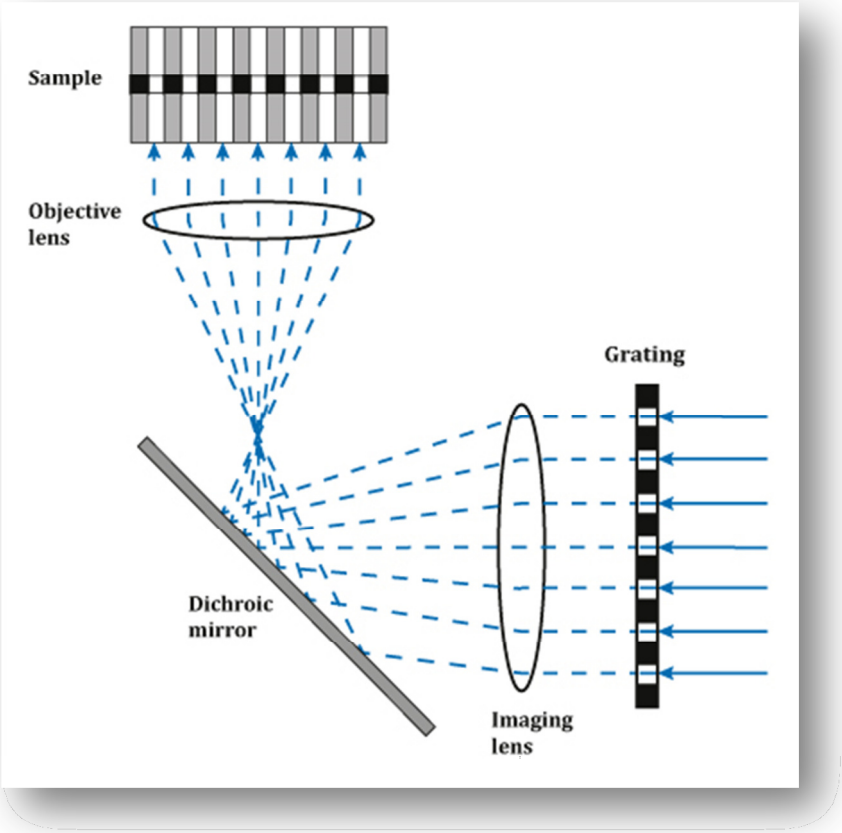

Figure 7 The concept of structured illumination (modified from Quercioli, 2011)

An optically sectioned image of the sample is achieved, thus with an undesired grid pattern superimposed, where the spatial frequency that is used to illuminate the sample affects the rate of attenuation with defocus or the strength of the optical sectioning. Assuming the illumination mask as a one-dimensional grid, the implementation of structured illumination is defined by the equation:

$$s_i(x,y) = 1 + m\cos(vx + \varphi_i) \tag{1}$$

The quantity *m* corresponds to the modulation depth, which is a measurement of the transfer of the illumination pattern contrast to the focal plan, that is related to the illumination frequency and scattering of the sample. The spatial frequency is represented by the quantity *v* and the phase shift of the pattern corresponds to φ_i. The sample illuminated by this pattern has a measured image intensity that can be described by following equation (Fu et al., 2013):

$$I_i(x,y) = d(x,y) + s_i(x,y)f(x,y) \tag{2}$$

The fluorescence emitted from the sample which is out-of-focus is represented by *d(x,y)* and *f(x,y)* is corresponding to the in-focus fluorescence. As seen in Equation 2, the sinusoidal component of the illumination pattern only modulates the in-focus fluorescence from the object and a proper demodulation method to extract only this information can be applied. A square-law detection in communication systems is the most commonly used algorithm to

demodulate and extract the in-focus component of Equation 2 (Neil et al., 1997; Fu et al., 2013):

$$I_{Sectioned} = \sqrt{(I_1 - I_2)^2 + (I_1 - I_3)^2 + (I_2 - I_3)^2} \quad (3)$$

In Equation 3, acquisition of three separate images (I_1, I_2, I_3) that are shifted in phase by φ_1= 0, $\varphi_2 = 2\pi/3$, $\varphi_3 = 4\pi/3$ determine the sectioned image $I_{Sectioned}$, containing the modulated part of the object that corresponds to the plane of focus (Fu et al., 2013).

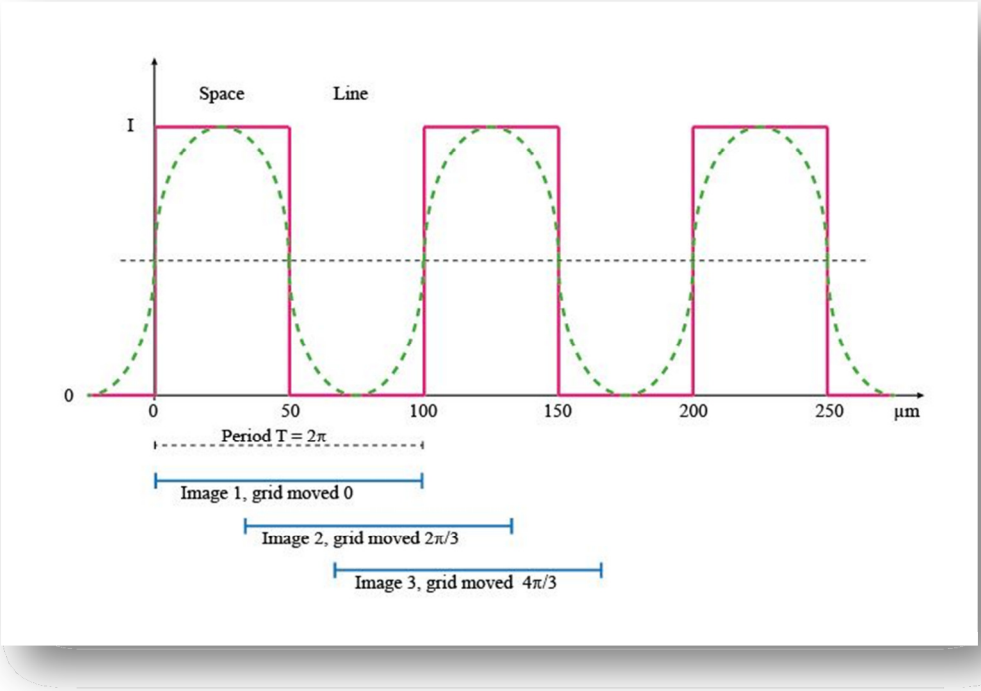

Figure 8 Grid pattern considered as a periodic function where movement of the grating causes phase shifts

The grid pattern can be considered as a periodic function, wherein one line and one spacing between two lines represents a period. At spacing, all light goes through and gives a maximum level of intensity (I). Where lines are present, no light pass and therefore give zero intensity, described as the red function in Figure 8. When moving the grid pattern in perpendicular direction to the lines, the same function arises but shifted in phase compared to the first function. The period is divided in equal number of steps to move the grid pattern as the number of images needed for the SIM calculation, which is denoted by the blue lines in Figure 8 where they are shifted 1/3 of the period for each of the three images. In Figure 9, an illustration shows three images, where the lines are shifted from each other.

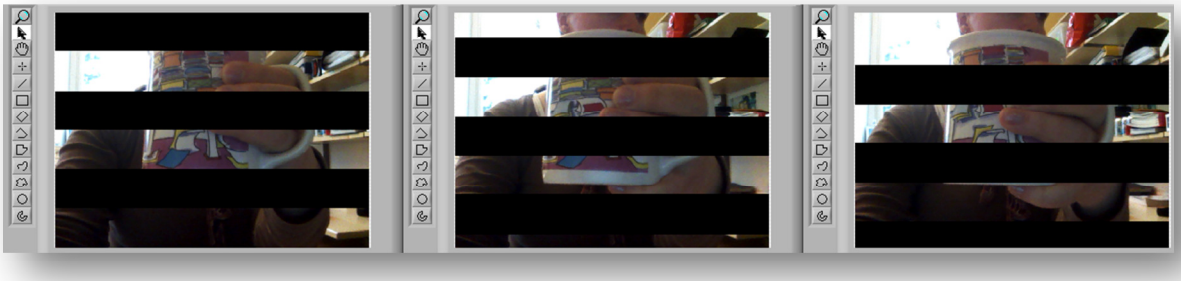

Figure 9 Three images with a grid pattern shifted by $\boldsymbol{\varphi_1}$= 0, $\boldsymbol{\varphi_2}$ = 2$\boldsymbol{\pi}$/3, $\boldsymbol{\varphi_3}$ = 4$\boldsymbol{\pi}$/3

One basic schematics of an experimental setup to acquire data from structured illumination is shown in Figure 6, where the illumination light is generated from a laser source. This setup is based on different kinds of lenses, a dichroic mirror, emission and excitation filter and a charge-coupled device (CCD) camera. The sample is illuminated by the illumination mask that produces a set of regularly spaced light patterns by shifting the mask with precise defined displacements. The scattered light or the fluorescence from the sample is then detected in the conjugate image plane, in a wide-field-type arrangement, where the CCD camera detects the image of the sample. This latter process is a common feature for all structured-illumination arrangements (Heintzmann, 2006; Schermelleh et al., 2010).

The illumination mask, which is a movable optical grating or grid, projects series of patterns of high spatial frequency onto the sample via the objective, see Figure 6. The pattern, typically of parallel spaced lines, is generated by a laser light passing through the mask, which then illuminates the sample with structured light (Heintzmann, 2006; Schermelleh et al., 2010). The use of patterned light is a well-established idea, and has been utilized when measuring surface shapes and deformations of cells. When considering axial or lateral resolution enhancement, a lateral light pattern has been considered to be a more effective approach to retrieve high-resolution information (Gustafsson, 2005).

Different SIM setups can slightly vary from each other depending on what kind of pattern generation used or on the detection system. The pattern can either be generated by a spatial light modulator (SLM) or an illumination mask (Heintzmann, 2006). The SLM modulates the intensity of the light beam and displays a computer-generated pattern (Hirvonen et al., 2009). In contrary, when a SLM is not used, the movement of the diffraction grating is mechanically moved, often by a piezoelectric actuator, where the mechanical movement of the grating can be somewhat slow compared to the use of the computer-driven SLM (Kner et al., 2009). The limitations in speed when using a piezoelectric actuator is caused by the need to stabilize before an image can be acquired in the incremental movements (Chasles et al., 2007).

2.3.2 Resolution

The reason SIM roughly can two-fold the resolution in its linear form is that high frequency structural information is shifted to within the detection range of the microscope by mixing the excitation pattern with the spatial information in the sample. The detectable frequency range of the microscope is therefore expanded by SIM which reduces the size of the PSF (Bates et al., 2008).

When nonlinearity appears between the intensity of the illumination and the measured emission intensity, even higher resolution can be reached, where fluorescence saturation is one kind of nonlinear effect. Saturated structured illumination microscopy (SSIM) uses this effect of saturation of fluorophores and it has been demonstrated that SSIM is possible to reach a resolution better than 50 nm. The saturation of fluorophores requires extremely high illumination intensity that can be achieved by the use of pulsed lasers and illumination of few nanoseconds (Heintzmann, 2006). However, the required high powers of the lasers in order to achieve saturation may lead to excessive bleaching (Schermelleh et al., 2010).

2.3.3 Other far-field methods

There are, as mentioned in the beginning of section 2.3, other modern super-resolution fluorescence microscopy approaches that are relatively new inventions. Stimulated emission depletion (STED) microscopy is one of them, and it is a scanning method in comparison with the non-scanning featured SIM. Methods based on localization, such as photo-activated localization microscopy (PALM) and stochastic optical reconstruction microscopy (STORM) are other recently introduced super-resolution methods (Kner et al. 2009).

STED microscopy is a nonlinear process, and it uses two synchronized ultrafast laser beams to scan through the sample. It takes advantage of the depletion of fluorophores from the excited state by stimulated emission. A second red-shifted STED beam is followed after the first focused excitation beam that pumps the fluorophores to their excited state. This added beam is typically doughnut-shaped, see Figure 10 B, in order to trigger stimulated emission of the excited fluorophores (Bates, M. et al., 2008). The resolution of STED from recent experiments has reached the range of 30 - 80 nm (Schermelleh et al., 2010). The drawbacks of using STED in some applications are that it requires precise control of two laser beams, such as the amplitude, phase and position of the lasers (Ji, N. et al., 2008). Also, its best resolution is restricted to certain dyes, and therefore an important consideration is the choice of right dye. The set of suitable dyes are limited compared with other conventional methods since appropriate photo-chemical properties are required (Schermelleh et al., 2010)

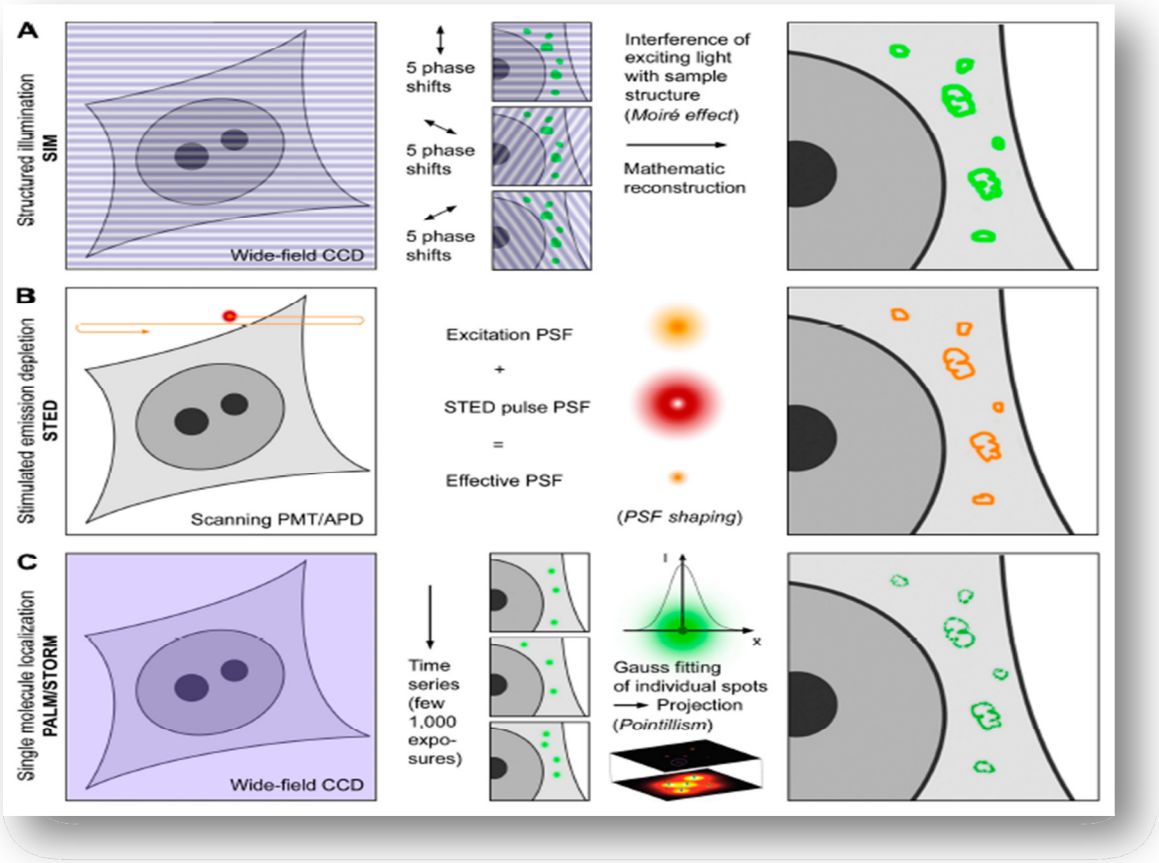

Figure 10 Comparison between STED, SIM and PALM (Schermelleh, 2010)

Methods based on localization, such as PALM and STORM can achieve extremely high resolution but are limited in speed since they require a large amount of raw images, almost hundreds to tens of thousands (Kner et al., 2009). These approaches also take advantage of a nonlinear effect that is caused by enhancing the emission PSF when combining many photons (Schermelleh, 2010).

2.4 Piezoelectric fundamentals

Piezoelectric positioning stages have become more and more used for nanometer displacement resolution in many applications due to the rapid development of nanotechnology and nanoscience (Gu et al., 2012). The following section will give a brief description of general piezoelectric positioning stages and an overview of the piezoelectric effect.

2.4.1 The piezoelectric principle and applications

The ability of a material to generate an electric charge when mechanical stress is applied defines the piezoelectric effect. The positive and negative charge of a material shifts when mechanical stress is applied, resulting in an external electric field. The piezoelectric effect has an extraordinary property of being reversible, meaning that a material also can exploit the inverse piezoelectric effect by generating a mechanical stress and/or motion when applying an electric field (Nanomotion, 2013).

The properties of the piezoelectric actuators are the main reason of the growing popularity of usage, *e.g.* fast response, compact size, zero backlash, fast oscillating motion, high output

force and high-precision motion displacements. The nano- or subnanometer displacements are highly desired features in many industrial applications, such in micromanipulations, intracellular manipulations and for auto-focusing systems in microscopes. Even though these motion stages attribute high precision, there are disadvantages to be considered. The relationship between input applied voltage and the desired output displacement is highly nonlinear. This is the major drawback, where the nonlinearity depends on the hysteresis effect and creep/drift effect. The desired high-precision motion accuracy and resolution is therefore somewhat limited (Gu et al., 2012; Liaw et al., 2007).

2.4.2 Model of general piezoelectric actuator

Based on recent studies (Liaw et al., 2007) a general electromechanical model of the piezoelectric actuator has been evaluated that consists of three stages of the transformation. The three stages include the voltage-charge stage, the piezoelectric stage and the force-displacement stage.

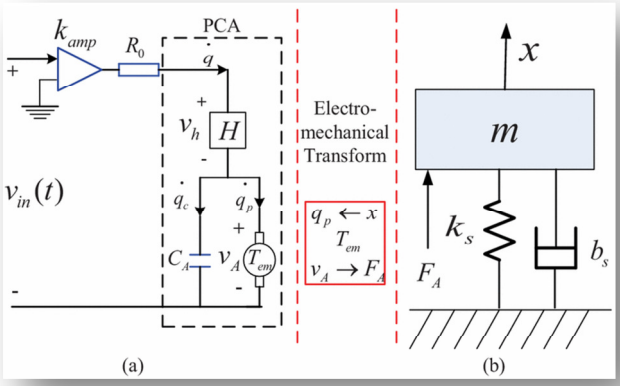

Figure 11 General model of a piezoelectric stage effect from an electrical (a) and mechanical (b) aspect (Gu et al., 2012)

Four components typically contribute to the piezoelectric positioning stage system: a piezoelectric ceramic actuator (PCA), a flexure-hinge-based mechanism, a piezoelectric driver amplifier (PDA) and a displacement sensor. The flexure-hinge-based mechanism contributes to motions that are created by elastic deformations of the stiff metal part. The large output force, fast response time and high bandwidth of the PCA allow it to generate a force on the mechanisms and therefore is a PCA applied to the stage system in order to realize the actuation function. The PDA is illustrated in Figure 11 as the gain k_{amp} and internal resistance R_0 and is supplying power to the PCA by charge control or voltage control. The real-time motion displacement of the stages is measured by the displacement sensor. The hysteresis effect is indicated by H in the figure, which generates the voltage v_h, and T_{em} corresponds to the piezo effect. The relationship between the electrical charge, $q_p(t)$, and the piezoelectrical effect, T_{em}, related to the output displacement of the actuator, $x(t)$, is expressed and evaluated by following equations (Gu et al., 2012):

$$R_0\dot{q}(t) + v_h(t) + v_A(t) = k_{amp}v_{in}(t) \tag{4}$$

$$v_h(t) = H(q) \tag{5}$$

$$q(t) = q_c(t) + q_p(t) \tag{6}$$

$$v_A(t) = \frac{q_c(t)}{C_A} \tag{7}$$

$$q_p(t) = T_{em}x(t) \tag{8}$$

The sum of the capacitances of the piezoelectric ceramics is represented by C_A and q_c is the stored charge in C_A. The control input of the PDA is expressed as v_{in}, the total charge in the PCA is represented as q and the current flowing through the circuit is $\dot{q}$. The damping coefficient, mass and stiffness of the moving mechanism are represented by b_s, m and k_s in the mechanical part (Gu et al., 2012).

3 Material and method

The methodology can roughly be divided into three parts; simulations with LabVIEW™, photo-lithography in order to fabricate the grating mask and completion of the optical table setup to achieve the SIM-images. The different parts were performed partly in this study, where the main part was programming and simulations of a piezo controller and actuator which was made to complete the system design of the optical setup.

3.1 Photo-lithography

Transferring a desired pattern onto a surface of a solid material is the principle of photo-lithography. This top-down approach is the most widely used in the field of micro- and nanotechnology due to its submicron accuracy. Photo-lithography involves several steps, where the first step, called spin-coating, covers a substrate with a photo-resist that can either be positive or negative (Figure 12). By spinning the substrate with the resist at high rates, a thin uniform resist coating can be achieved that depends on spin rate, duration and type of resist. Built-in stresses in the resist coating may appear after this step since the resist still may contain up to 15% solvent. These stresses can be reduced by evaporation of the solvents by the following step called prebaking, sometimes also known as soft baking (Madou, 2002).

An exposure system including exposure and alignment of the substrate is the following step, where the substrate will be aligned with the desired pattern on the mask and thereafter exposed by *e.g.* an UV lamp. The purpose of exposure is to transfer the mask image perfectly onto the resist, obtained by illuminating the resist with proper density, exposure time, wavelength and directionality. When the resist has been exposed, it needs to be developed, which means dissolving of the photo-resist, typically done with a chemical developing solution. Next step before etching, the substrate needs to be postbaked depending on what kind of etch method that will be used. Postbaking improves the hardness of the film due to increased photo-resist resistance when etching. The last step is the complete removal of the photo-resist, called photo-resist stripping, where a solvent is used to remove the unexposed resists on the substrate (Madou, 2002).

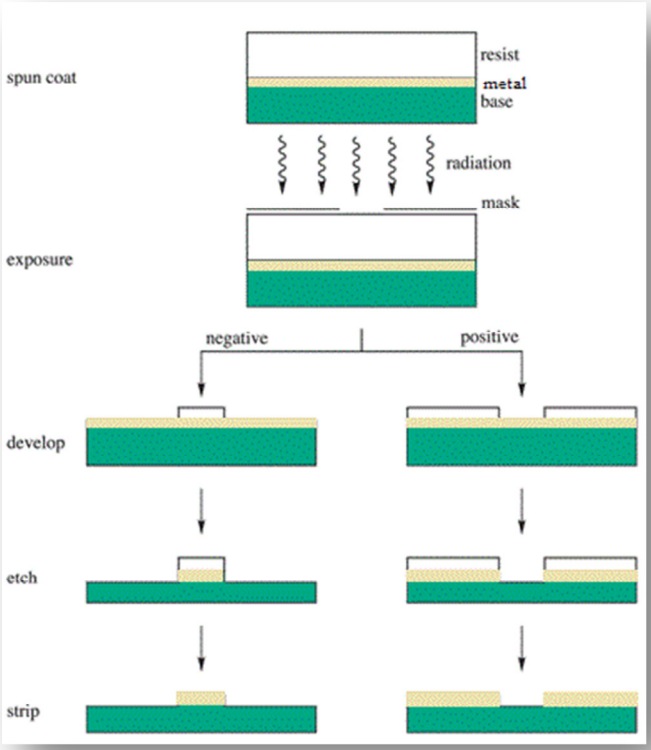

Figure 12 Photo-lithography process (Sigma-aldrich, 2013)

Photo-lithography was used in this study to fabricate the grid pattern on glass cover slips of size 20 x 20 mm. The photo-lithography was performed in order to transfer the desired pattern onto the cover slips that will become our grating mask. The critical aspects of the final mask is of being a high degree of line opacity, with an optical density (OD) of at least 5, while maintaining a sharp regular line boundary, with variances no greater than 500 nm. Optical density is a logarithmic ratio of intensity between incident and refracted light, that is determined by $-\log_{10}(I_{out}/I_{in})$. The higher value of the OD of a material, the less transmittance is the material. An optical power meter (FieldmaxII, Coherent Inc.) was used to measure the OD of the metal layers. The process of photo-lithography follows a recipe to achieve the desired properties of the patterned mask. The recipe used in this study is presented in Appendix A.

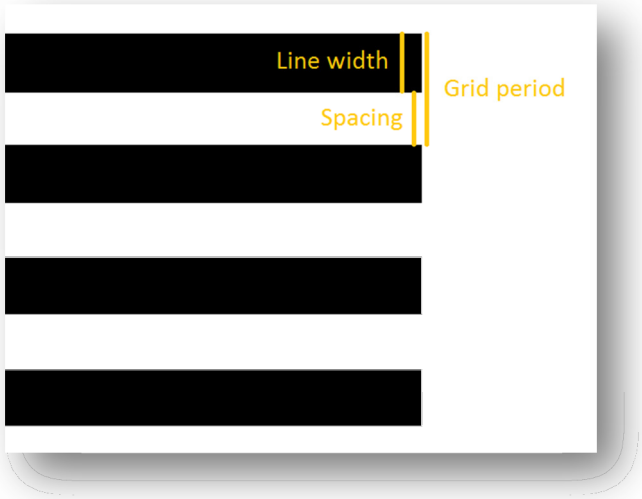

Figure 13 Illustration of the grid pattern

The cover slips used were of pure white glass squares of hydrolytic class I and they were ordered from *www.vwr.com*. The grid period of the grating, see Figure 13, is twice the size of the horizontal line width, *e.g.* a line width of 50 µm has a grid period of 100 µm. The different grid periods, *i.e.* the different periodical length of the line spacing, are drawn since they depend on what sample that will be studied and what kind of chosen objective that is used in the microscope. A mask design with ten different characteristics was drawn in AutoCAD®, seen in Figure 14, for ordering a chrome on glass mask from the company *www.jdphoto.co.uk*.

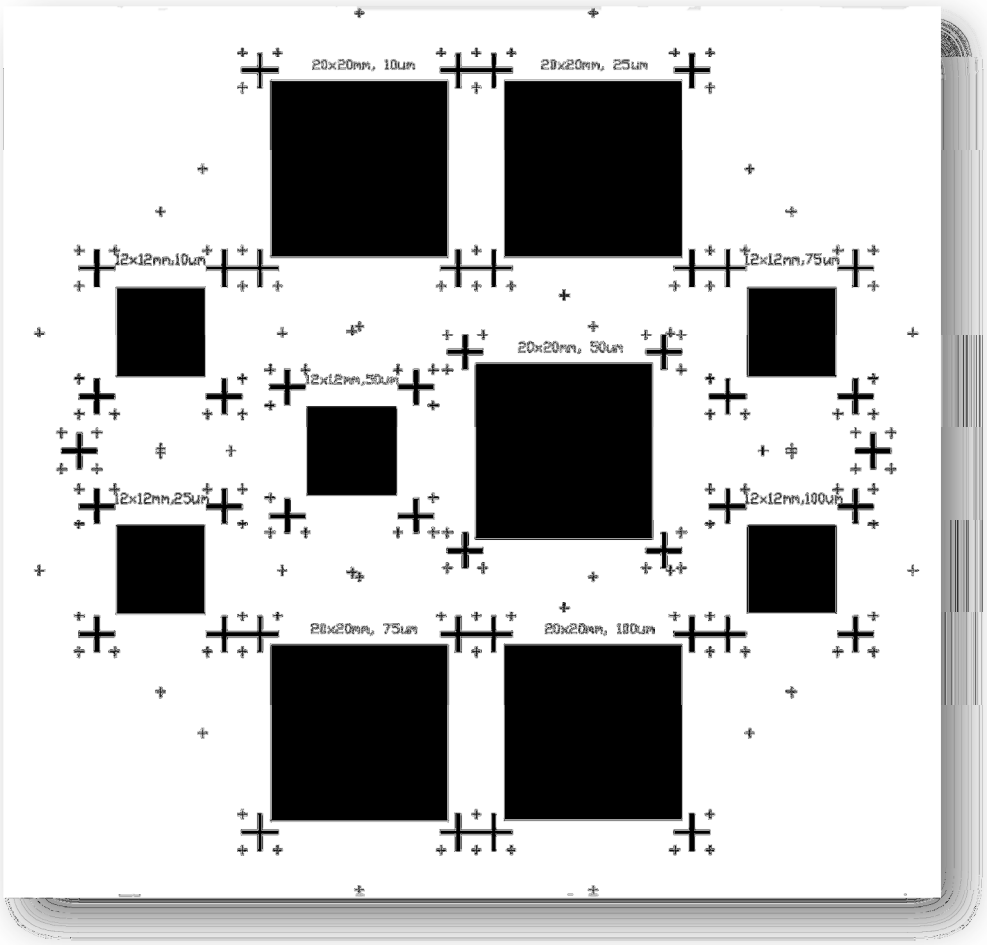

Figure 14 Mask design with ten different features

Gold on titanium (Ti/Au) or aluminum (Al) were the metals deposited on the cover slips before photo-lithography. A Ti/Au layer of 300 nm and Al layer of 120 nm were studied to conclude what metal was most adequate for our grating mask. The thickness layer of the metals was calculated dependent of the metal properties in order to achieve appropriate opacity. Ti was a thin adhesion layer for the Au deposition in order to minimize adhesion problems.

3.2 LabVIEW

The recorded images were acquired using a custom made program in LabVIEW™ version 9.0 (32-bit), whereby the program interfaces between the camera and the piezo actuator position. The program was written such that the movement of the piezo actuator moves a stepwise distance of 1/3 of the mask pattern period and when the desired position is achieved, the LabVIEW™ program (see Appendix C) synchronizes with the camera to capture that position. The first position that is captured is at the initial place of the mask and the last position is captured in the same manner when the actuator has reached 2/3 of its initial state, which also is the final placement, and moving back 1/3 again to thereafter reach the initial state. Repeatedly, this movement of the actuator should continue in a frequency of 100 - 200

Hz, corresponding to approximately 10 - 50 ms, in order to *e.g.* capture moving cells as in this thesis.

The piezo controller and the piezo actuator were ordered from *www.thorlabs.com* and the requirement of the actuator was such that it was designed for critical alignment applications in nanometer motion control. A single channel piezo controller (BPC301) is used in this project with a piezo actuator with strain gauge feedback (PAZ015). The controller can deliver up to 150V/500 mA and the maximum travel length of the actuator is 100 μm and has a working voltage of 75 V. The controller is supplied with appropriate APT software, a tool which was used to simulate the written LabVIEW™ program before experiments. LabVIEW™ is supported by a Windows®-based, language-independent technology called ActiveX®, which provides necessary APT system software services to the LabVIEW™ program. This language consists of several methods which can be used to synchronize the controller and the LabVIEW™ program to acquire appropriate data from the actuator, *e.g.* desired position versus real position of the actuator. The specifications for the actuator were such that it cannot move faster than approximately 167 Hz and the slew rate for the actuator is maximum 25 V/ms. However, the requirement of the interval of 100 - 200 Hz is still fulfilled with this limitation.

Simulations to confirm the SIM calculations were programmed in LabVIEW™ (see Appendix B) by overlaying iterated horizontal lines shifted 2/3 from each other. The calculations were then applied to the images where a modulated SIM image could be achieved. An illustration of the program can be seen in Figure 15.

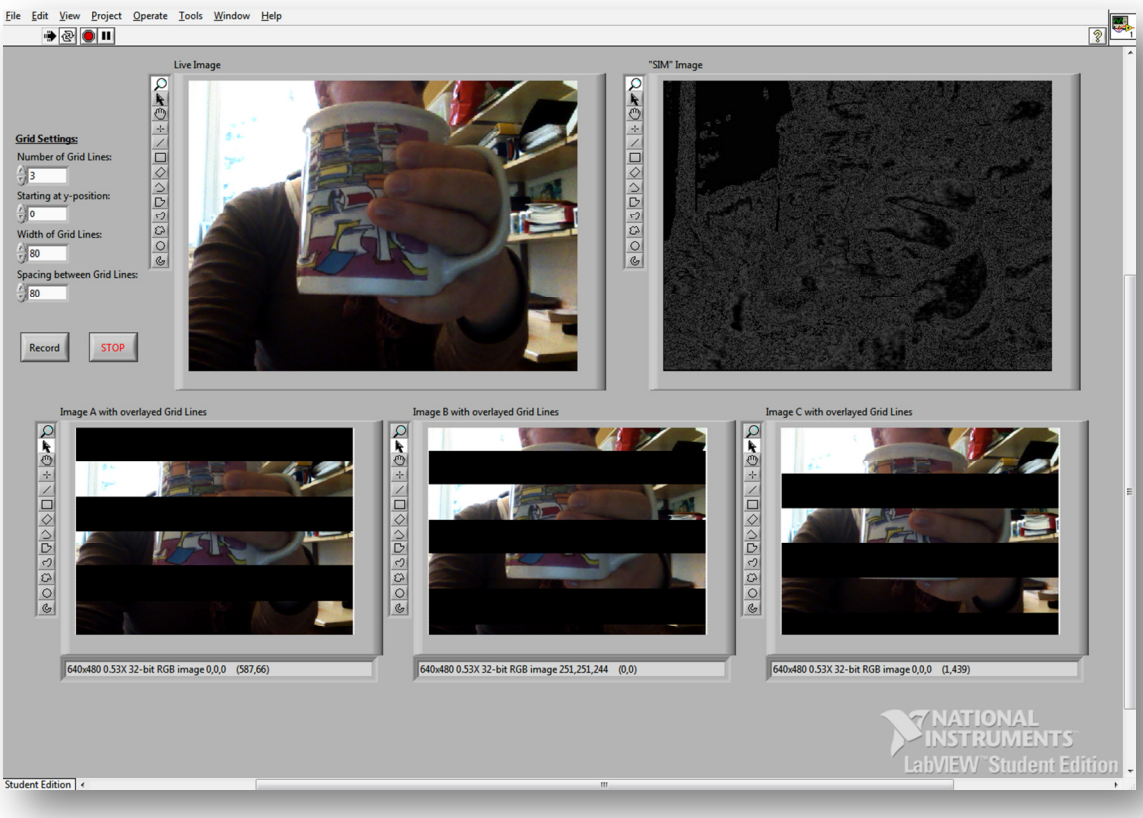

Figure 15 Interface of the program where overlayed lines shifted from each other were SIM modulated

3.3 Cell Culture

Studies on Human Embryonic Kidney (HEK) 293 and Chinese Hamster Ovarian (CHO) cells were performed in order to investigate if the microscopy method could achieve high resolution images. Human Embryonic Kidney (HEK) 293 cells were cultured in Minimum Essential Medium (MEM) with Earle Salt in a glass dish of 50 mm diameter until harvested (a density of approximately 50 000 cells/cm^2). Before the experiments, the cells were washed and an extracellular buffer (ECB) buffer replaced the culture medium, consisting of 140 mM NaCl, 1 mM $CaCl_2$, 10 nM D-glucose and 10 mM HEPES. Finally, the pH was adjusted to 7.4 with NaOH.

The CHO cells were cultured in flasks with growth medium HAM's F12 medium with 10% Fetal Bovine Serum (FBS) and L-glutamine (2 mM) incubated at 37° and 5% CO_2. Doxycycline (1 µg/ml) was used to activate the Transient Receptor Potential Vanilloid 1 (TRPV1). The chemicals used for cell culturing were ordered from PAA Laboratories GmbH, Paching, Austria.

The HEK 293 cells were labeled with Deep Red Plasma Membrane Stain and the CHO cells were labeled with FM1-43. These dyes were purchased from Life Technologies.

3.4 Multifunctional pipette

A multifunctional pipette (Ainla, 2010) is a microfluidic device, which is illustrated in Figure 16 below, and was used to deliver solutions to the CHO cells during the experiments. Four different solutions were added to the channels of the multifunctional pipette; Fluorescein (20 µM), as a fluorescent flow tracer, Capsaicin (10 µM) to activate the ion channel, ECB, a buffer for cleaning the cells and Yo-Pro-1 (1 µM), a fluorescent DNA intercollator dye for monitoring the reaction kinetics. Fluorescin is a fluorescent dye, Capsaicin is a strong activator of TRPV1 and is a compound in chili and Yo-Pro-1 is a nucleic acid stain that fluorescence when it bonds to organelle DNAs, such as small amounts of DNA that are present within the mitochondria for animals, plants and fungi (Lodish et al., 2000). During the experiment when the grid pattern was automatically moving by the piezo controller, the cells were exposed at different amount of times by the solutions.

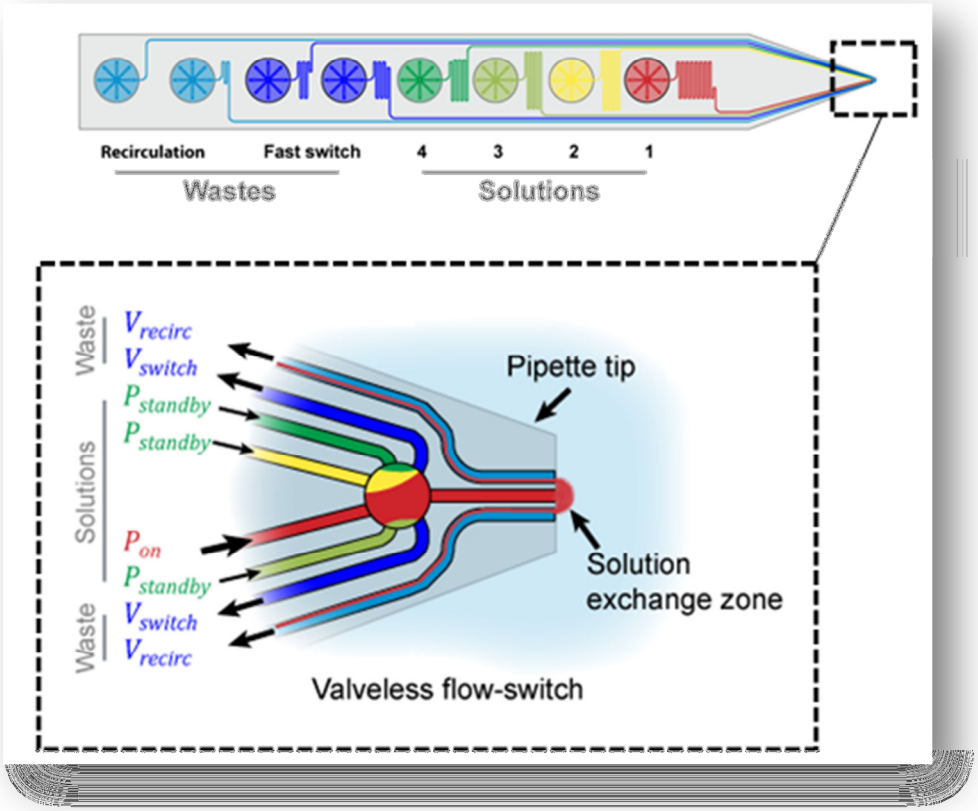

Figure 16 An illustration of the multifunctional pipette (Ainla et al., 2013)

3.5 Optical setup

An inverted fluorescence microscope (Leica DMIRB2, Leica Camera AG) was used for all experiments, where the optical setup to achieve SIM-images is a compilation of experiments with various kinds of lasers, lenses and mirrors. In the Biophysical Technology Lab, the fixed parts mounted on the optical table were the telescope and the imaging lens, where tube lens, grating, piezo actuator and mirrors were aligned with the laser beam. A schematics of the optical setup is illustrated in Figure 17. The cube assembly consists of a dualband dichroic letting wavelengths of 488 nm and 1064 nm reflect. There is no excitation filter and the emission filter is a longpass filter allowing wavelengths over 515 nm pass.

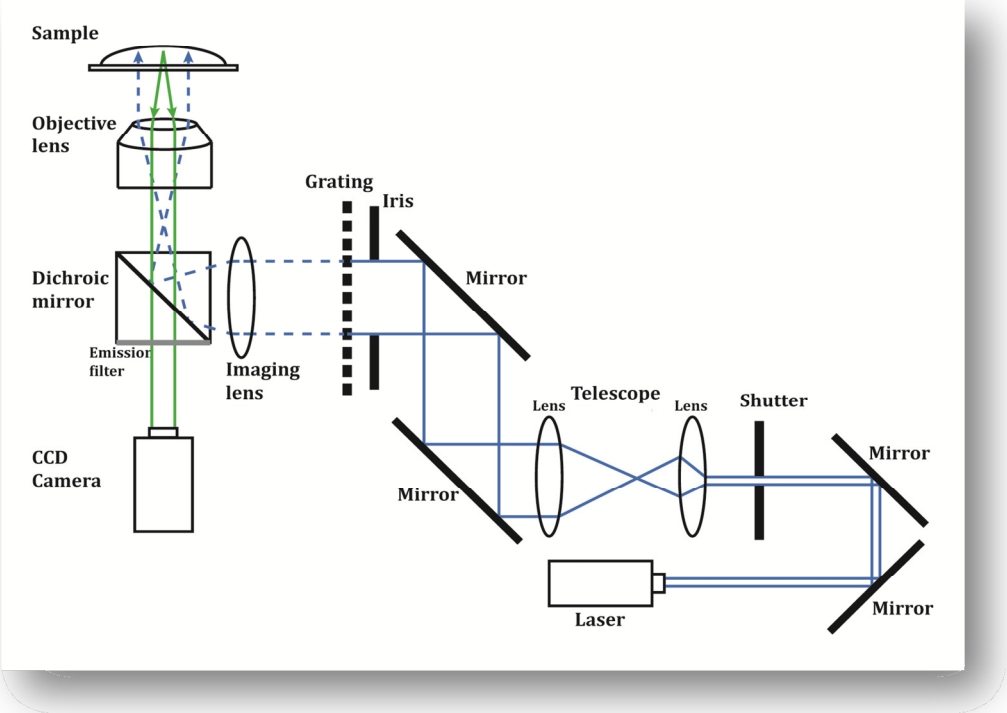

Figure 17 Schematics of the optical setup

Before experiments on living cells with the fabricated grating, studies were performed on a thicker and fixed sample, a lily root (thickness ~ 100 - 150 μm) with antibody stain with a static pattern mask with grid line size of 50 μm and grid period of 100 μm. A Ti-Saphire laser was used (λ = 488 nm) and alignment of the beam was directed to the very center of the grating. This was performed by tweaking and adjusting the imaging lens and tube lens simultaneously while observing and directing the laser beam to desired targets at the walls.

An objective of 20X with air and NA = 0.75 was used, and when observing the lily root, unexpected dark structures appeared in the image detected by an 8-bit CCD camera (gx1920, Allied Tech). To eliminate these unwanted dark structures on the image, some standard cleaning of lenses and mirrors was done. The images of the lily root were recorded by the CCD-camera where the movement of the grating was manually moved with a micrometer with a speed of approximately 10 microns per second. In this step, a cover slip with grid period of 200 μm was used. The record of this manual movement was analyzed by extracting three images in the movie where the grid pattern was moved one third from its initial state twice.

Studies of HEK 293 cells were studied with a 40X objective with immersion oil and NA = 1.25. The setup is otherwise same as the experiment on the lily root and the movement of the grating had the same procedure.

The experiments on the CHO cells had the same setup as previous experiments, and were performed with a 40X objective with immersion oil and NA = 1.25. The movement of the

grating is instead controlled automatically by a piezo actuator. The piezo actuator was mounted such that the grating could move up and down. Tack-it was used to mount the grating onto the piezo actuator.

4 Results

Observing the metal deposition after the steps of the photo-lithography process, Al was the deposition metal that was chosen for grating fabrication due to a smaller thickness of the deposition layer was needed compared to Au. In Figure 18 below, a comparison between the Al and Au deposited on cover slips are presented. In the left picture, the Al deposited cover slip can be seen where the grid period is measured to 100.49 µm and 99.65 µm. The size of the grid line is measured to 46.48 µm, *i.e.* smaller than the desired size of 50 µm. The Au deposited cover slip is shown in the right picture, where it can be seen that the space between the lines is broader, due to over-etch. The grid period here is measured to 100.07 µm and 100.49 µm, but the line sizes are small as 32.25 µm and 32.24 µm.

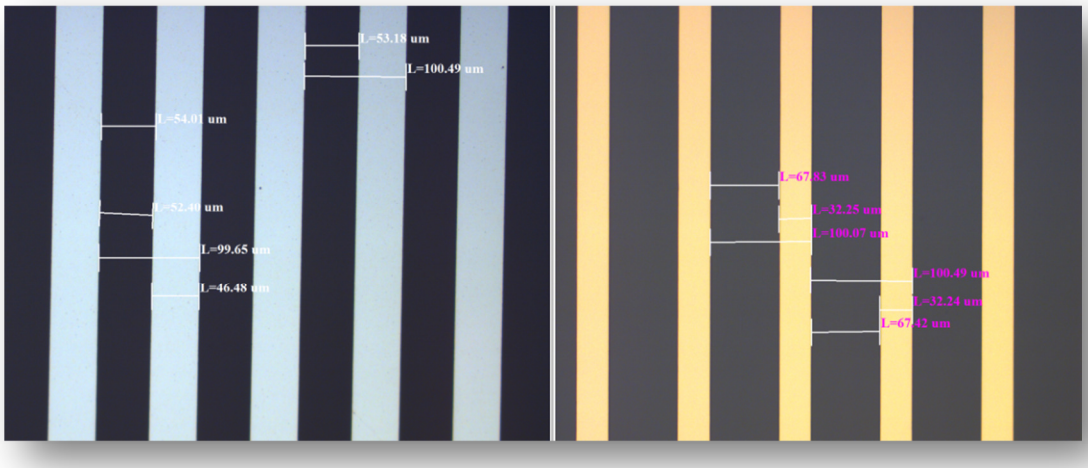

Figure 18 Comparison between Al (left) and Au (right) deposited cover slip

Even though over-etching was observed, a comparison of the opacity of the both metals deposited on the cover slips was performed by illuminating them with a laser beam. The OD could be then be calculated, where OD for Al was calculated to 6.1 and for Au calculated to 4.1. The requirement of OD of the deposited metal is 5 or higher, thus was Al chosen since it was measured to OD > 5 when the thickness of Al was 120 nm. Au was therefore not chosen as the deposition metal due to the larger amount of metal needed compared to Al. The optical power measurements are presented in Table 1.

Table 1 Optical power measurements of glass cover slips deposited with Al and Au

Metal	Thickness [nm]	Power In [W]	Power Out [W]	Ratio (%)	OD
Al	90	4.3 * 10^-3	6.5 * 10^-8	1.5 * 10^-3	4.8
Al	120	4.0 * 10^-3	3.0 * 10^-9	7.5 * 10^-5	6.1
Al	150	4.0 * 10^-3	n/a	n/a	n/a
Ti/Au	300	5.3 * 10^-4	4.4 * 10^-8	8.3 * 10^-3	4.1

As seen in Table 1, all thicknesses of Al layer reached the requirement of OD > 5. Al with the layer thickness of 120 nm will be used in this thesis, due to higher OD than for the one with 90 nm thick layer. The OD for the thickness of 150 nm Al resulted in inconsistent values due to fluctuating values on the instrument due to inconvenience in thickness where the surface were not regular. The thickness of the Al and Au deposited cover slips were measured by a surface profiler where the thickness of the Al layer was measured to an average thickness of 113.20 nm, which should have been 120 nm. The average thickness of the Au layer was measured to 346.65 nm, which was expected to be 300 nm. These results show that inaccuracy when depositing the metal on the cover slip by a sputtering method might affect OD.

Three images from the experiments with the lily root were read into the LabVIEW™ program. SIM calculations were made in order to see if the modulated image could achieve higher resolution with structured illumination calculations, see Figure 19, where the scale bar indicates 500 µm.

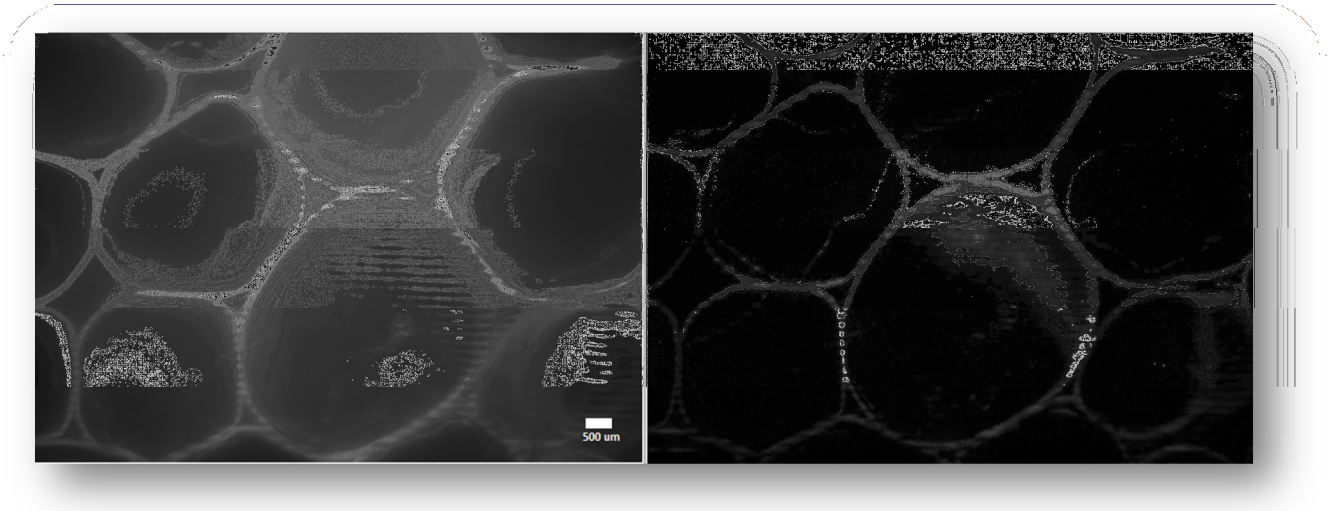

Figure 19 Comparison of an image with out-of-focus fluorescence (left) and structured illuminated modulated image (right) with reduced out-of-focus fluorescence

As seen in the figure, the modulated image (right) has a reduction of out-of-focus fluorescence compared to the original image. However, the modulated image still contains horizontal lines, an artifact likely due to a manual positioning error of the grating during the analysis.

In the experiments on HEK 293 cells, investigations with a smaller grid period were performed. It turned out that it was difficult to extract raw images for SIM calculations when using the grid period of 50 µm since the grid line was not clearly distinguished, see Figure 20. However, when trying to extract images with correct displacement of the lines, the modulated SIM image still had reduced out-of-focus fluorescence, but with artifacts of horizontal lines, larger than the previous experiment when using a 200 grid period.

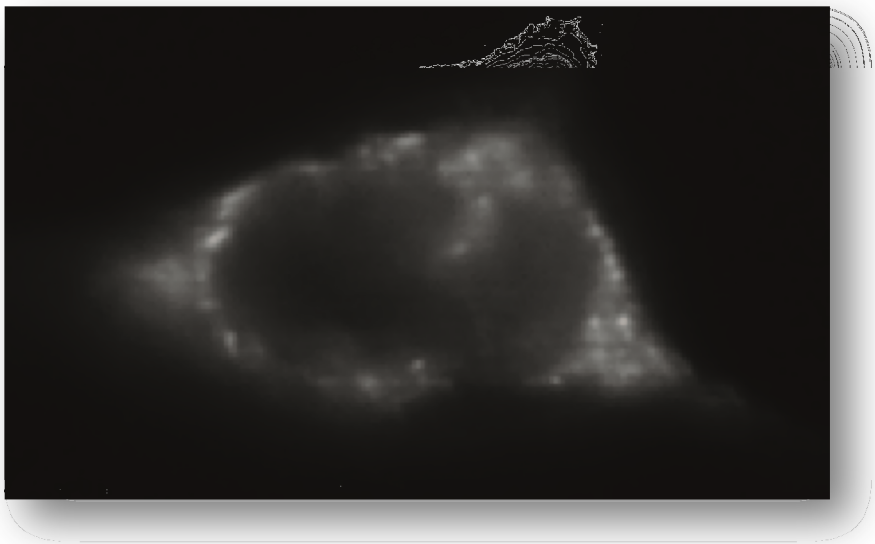

Figure 20 Raw original image of HEK 293 cells with a grid period of 50 µm

The final experiments with the piezo actuator implemented were performed on CHO cells, where the cells were probed with the solutions by the multifunctional pipette. A mask pattern with a grid period of 100 µm was used and the step length of the piezo actuator was measured to travel one third of 100 µm, *i.e.* from 0 µm, 33 µm, 67 µm and 100 µm, where the camera captured the positions of the piezo automatically, by putting in the same delay as the piezo controller had for each step, here approximately 1.305 ms. In Figure 21, two plots of the piezo stepping are presented for two different time delays; 300 ms (left) and 4000 ms (right). As can be seen, the desired positions are not reached with the smaller delay due to that it gets a new value from an array with desired positions before it actually reaches the previous position.

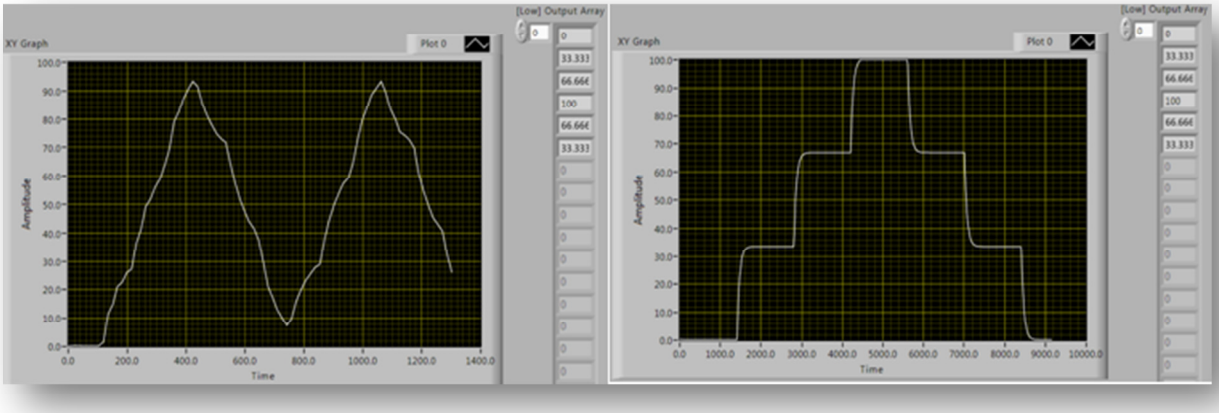

Figure 21 Comparison between responses for a piezo step with different time delays

The real optical setup is shown in Figure 22 A, where the place of the piezo actuator is indicated by the yellow arrow. Different lenses and mirrors can be seen and the microscope part is placed behind a black cardboard shield and therefore not visible in this image. The piezo actuator was mounted, as seen in Figure 22 B, such that the grating was stepped from up to down due to that the length of the actuator was too long to be mounted on the table. An iris

to narrow the laser beam is seen in front of the grating and the mass of tack-it that holds the grating on the actuator is pointed out by the arrow.

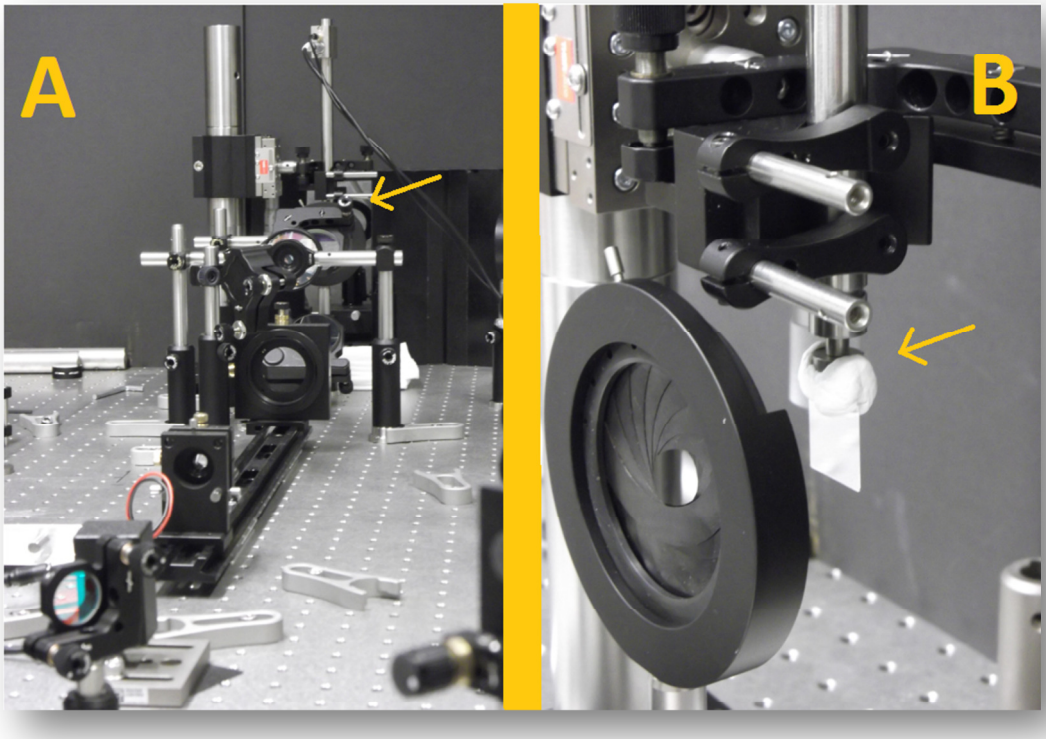

Figure 22 Optical setup A) arrow indicating placement of piezo actuator and B) close-up of the up-side-down piezo actuator with the grating mounted with tack-it

5 Discussion

The constructed SIM images from the experiments of the cells resulted in an improved image quality due to the reduction of the out-of-focus fluorescence in the original images. However, the final SIM images still contained horizontal lines, which should be fully eliminated in the SIM image according to equation 3 in Section 2.3.1. Simulations with overlayed horizontal lines, seen in Figure 15, resulted in an output image with no horizontal lines. Due to this, we confirmed that the SIM calculations should give an output image without lines in our experiments. Since the lines in the SIM image from our experiments were not fully eliminated, we concluded that several error sources could contribute to this artifact.

The mass of the mounting with tack-it has no major effect on the piezo actuator since it can tolerate a mass of up to tens of kilos, but the amount of mass holding the grating is rather significant. A larger mass of tack-it is needed in order to reduce deflections of the cover slips when fast movements of the piezo actuator are achieved. Due to that tack-it is not rigid; deflections still may appear when moving the cover slips at high speed. The mounting of the piezo actuator on the optical table was mounted top-down wise, which might affect the stability of the grating when attached on the piezo actuator over longer time due to stress on the tack-it. The size of the glass cover slips has also been in mind, since deflections of the cover slip may appear for larger pieces of cover slips. In this study, only one size, 2 x 2 cm, were examined in the experiments

The different sizes of line and grid periods on the cover slips were fabricated mostly due to exploit what kind of sizes that are proper to work with. It turned out that a grid period of 100 μm was most suitable from the grid periods fabricated in this study when having maximum travel length of 100 μm of the piezo actuator. Grid periods smaller than 100 μm were not used since it was difficult to distinguish the accurate displacement of the grid pattern when having too small lines when performing the first experiments. However, using a grid period of the same as the maximum stepping length of the actuator is not the best solution, since the actuator may not reach the desired position at higher speeds. By using a smaller grid period compared to the maximum step length, the desired position may be reached by setting a higher voltage than expected to reach the exact position.

When observing the grid periods after fabricating the gratings, it was seen that the size of the lines had small variations on the cover slip, mainly due to over-etching. The lines were smaller than expected and this inconveniency may contribute to horizontal lines in the SIM image.

Since synchronization between the camera and piezo position was not succeeded, a delay in camera capturing a sequence of images was required. When synching the desired position and camera, by setting a capture delay as the same as the calculated delay time of the piezo actuator, a synchronization error still may occur due to not exact delay times. By visual observations on the piezo controller, manual capturing of the images in the positions could be performed. This resulted in thinner lines in the SIM images. It is a better result compared to the one when putting in an automatic capture delay, but it still contained lines which means that the synchronization is not the only error source.

Investigations of strategies to trigger the synchronization were performed. The first attempt was to use the software trigger, where in-built functions in the software were studied in order to observe the triggering possibilities. It was found out that the triggering for each position could not be achieved. But it was possible to trigger once or several times within an array of positions, except for the first element in the array. Due to this, the triggering for each desired position was not achieved since every element in the array is a desired position, and another strategy to trigger had to be analyzed. Therefore, an oscilloscope, which has an in-built trigger out function, was used via the piezo communication line to see the response of the piezo actuator stepping in real time. From this observation, trigger out could be set dependent on either the rising or the falling slope of the stepping curve. However, this strategy was not tested on the real setup to trigger the synchronization between the camera and the piezo controller. Other alternatives have been discussed, such as an optical sensor could for example be added to the optical setup, which will collect the reflected light when the laser beam is hitting the grating at the different positions. The light is reflected since the metal coating of the grating acts as a mirror. The amount of reflected light for the different desired positions of the grating is measured in voltage. This signal could then be sent to logic gate circuits where signals of variable voltages only will be considered as two types of signals; high (1) or low (0). Standard transistor-transistor logic (TTL) operates with 5V +/- 0.25V, a common voltage for trigger signals. TTL gates consider signals in ranges of voltages to be either high or low. These ranges also differ for TTL input signals and TTL output signals, where the output ranges are narrower than the input ranges and the range in between is the noise margin of the gate (All about circuits, 2012). From this, a triggering could be achieved when measuring the amount of reflected light for the desired positions of the grating and then trigger the camera to capture.

A SIM calculation of five images instead of three images was also investigated, in order to see if it would improve in resolution or the reduction of the horizontal line artifacts. But no significant improvements were found, so three images are adequate for the improved resolution.

6 Conclusion

- The constructed SIM images from the experiments of the cells resulted in an improved image quality due to the reduction of the out-of-focus fluorescence in the original images.

- The calculations in order to achieve a SIM image were confirmed by simulations and therefore concluded to work.

- Five images gave no significant improvement, so calculation from three images was concluded to be adequate.

- Higher speeds of the piezo controller were not tested due to that the synchronization of the camera and the piezo was not succeeded. A conclusion of how proper tack-it works as mounting material could therefore not be drawn, since there was no fully elimination of lines in the SIM images at low speed and the fixation of the grating was not stressed at high speed over longer time.

- The dependency of the coverslip mass was not investigated since only one size was used.

- Since improvements in line elimination were achieved when synching manually at slow speed, a conclusion that the synchronization failure was most likely not the only error source contributing to line appearance.

- This setup was concluded to be a cost effective solution, since it could be implemented on an existing fluorescence microscopy setup when synchronization is succeeded and when improved fabrication of the grating is achieved.

7 Future work

There are several possibilities that can be done to optimize the modulated images. Primarily, the horizontal lines in the SIM image need to be fully eliminated. This error may be solved by get higher accuracy of the line size on the glass cover slips when fabricated. Also, when fabricating the grating, a suggestion can be to use another lithography method, *e.g.* e-beam or laser writing.

An improvement in this study would be to get the synchronization between the piezo actuator and camera to work. Optimization of the synchronization could be investigated, which was mentioned in the discussion, by adding an optical sensor to the optical setup to trigger the camera based on where the grating is placed.

The mounting material that was used in this study in order to hold the grating was tack-it, which is not so rigid. When choosing mounting material, a suggestion can be to use a more hardening type of tack-it which might reduce deflections of the cover slips. Another suggestion is to design a holder in plastic for the cover slips, for example by a 3D printer. With a good design of this holder, it may also result in possibilities of changing between different gratings easily.

Due to our limitations when placing the piezo actuator, we chose to move the grating in a top-down direction. It would therefore be interesting to see how the opposite direction of the movement of the grating affects the proper displacement. The grating could also for example move in a horizontal direction instead of vertical.

It would be interesting to investigate if another piezo controller or another program is more suitable for this application in comparison to those used in this study.

Acknowledgement

First, we want to express our special thanks of gratitude to our supervisors Aldo Jesorka and Gavin Jeffries which gave us the opportunity to do our Master's Thesis in your team. We really enjoyed our time at your lab and thank you for giving us experiences in areas outside our biomedical field.

Aldo, thank you for the guidance and motivations you've contributed with. We are very grateful!

Gavin, thanks for all the patience you had when helping us through the whole work and all advices and knowledge you brought to our life. We couldn't be more thankful!

Jonas Fredriksson, who supported us with your ideas and knowledge! We want to thank you and we are very happy that we got the opportunity to have you as our examiner.

To all past and present members of the Biophysical Technology Lab during our stay, thanks for taking care of us. Special thanks to Anna Kim who helped us a lot in the cleanroom and for lots of laughs and advices at the office. Kyril Kustanovich and Alar Ainla, thank you for helping us in the cleanroom. Also, thanks to Shijun Xu who introduced us to the cell lab and for helping us with our cell experiments.

We would also like to express our gratitude to the MC2 Cleanroom staff; especially Ulf Södervall, Johan Andersson and Göran Alestig for helping and guiding us.

Last but not least, we would like to thank our family and friends for all support and encouragement. Especially, big thanks to David Boman for being supportive and a good "bollplank", Ulf Södervall who introduced us to the Biophysical Technology Lab, Stellan Karlsson who let us borrow an important part that brought us forward in our study and Thomas Jansson for being supportive and understanding.

References

Ahemaiti, A. (2010) ‘Effect of membrane composition on temperature activation of TRPV1’ [2013-11-22]

Ahemaiti, A., Ainla, A., Jeffries, G. D. M., Wigström, H., Orwar, O., Jesorka, A. & Jardemark, K. (2013) ‘A multifunctional pipette for localized drug administration to brain slices’ [2013-11-26]

Ainla, A., Jansson, E. T., Stepanyants, N., Orwar, O. & Jesorka, A. (2010) ‘A Microfluidic Pipette for Single-Cell Pharmacology’ [2013-06-03]

All about circuits (2012) *Logic signal voltage levels* Available from: <http://www.allaboutcircuits.com/vol_4/chpt_3/10.html> [2013-12-20]

Bates, M., Huang, B. & Zhuang, X. (2008) ‘Super-resolution microscopy by nanoscale localization of photo-switchable fluorescent probes’ *Current Opinion in Chemical Biology* pp.505-514 [2013-05-20]

Chasles, F., Dubertret, B. & Boccara, A. C. (2007) ’Optimization and characterization of a structured illumination microscope’ [2013-05-14]

Conchello, J. & Lichtman, J. W. (2005) ‘Optical sectioning microscopy’ [2013-05-14]

Fu, H. L., Mueller, J. L., Javid, M. P., Mito, J. K., Kirsch, D. G., Ramanjuam, N. & Brown, J. Q. (2013) ’Optimization of a Widefield Structured Illumination Microscope for Non-Destructive Assessment and Quantification of Nuclear Features in Tumor Margins of a Primary Mouse Model of Sarcoma’ [2013-08-26]

Gu, G., Zhu, L., Su, C. & Ding, H. (2013) ’Motion Control of Piezoelectric Positioning Stages: Modeling, Controller Design, and Experimental Evaluation’ [2013-07-31]

Gustafsson, M. G. L. (2005) ’Nonlinear structured-illumination microscopy: Wide-field fluorescence imaging with theoretically unlimited resolution’ [2013-05-06]

Heintzmann, R. (2006) ‘Structured illumination methods’ in *Handbook of Biological Confocal Microscopy*, 3d edition, Pawely, J. B., Springer US. pp. 265-279

Hell, S. W., Dyba, M. & Jakobs, S. (2004) ’Concepts for nanoscale resolution in fluorescence microscopy’ [2013-05-10]

Hirvonen, L. M., Wicker, K., Mandula, O. & Heintzmann, R. (2009) ’Structured illumination microscopy of a living cell’ [2013-05-07]

Jesorka, A., Stepanyants, N., Zhang, H., Ortmen, B., Hakonen, B. & Orwar, O. (2011) ’Generation of phospholipid vesicle-nanotube networks and transport of molecules therein’ [2013-06-03]

Ji, N., Shroff, H., Zhong, H. & Betzig, E. (2008) ‘Advances in the speed and resolution of light microscopy’ [2013-05-13]

Kner, P., Chhun, B. B., Griffis, E. R., Winoto, L. & Gustafsson, M. G. L. (2009) 'Super-resolution video microscopy of live cells by structured illumination'

Kohl, T., Westphal, V., Hell, W. S. & Lehnart E. S. (2012) 'Superresolution microscopy in heart - Cardiac nanoscopy' [2013-08-01]

Liaw, H. C., Shirinzadeh, B. & Smith, J. (2007) 'Enhanced sliding mode motion tracking control of piezoelectric actuators' [2013-07-31]

Lodish, H., Berk, A., & Zipursky, S. L. (2000), *Molecular Cell Biology*, 4th edn, W. H. Freeman, New York

Madou, M. J. (2002), *Fundamentalsof microfabrication: The science of Miniaturization*, 2nd edn, CRC Press, Boca Raton, Florida

Nanomotion, 2013, *The piezoelectric effect*, Available from: <http://www.nanomotion.com/piezoelectric-effect.html> [2013-09-04]

Neil, M. A. A., Juškaitis, R. & Wilson, T. (1997) 'Method of obtaining optical sectioning by using structured light in a conventional microscope' [2013-05-14]

Nogawa, K., Tagawa, Y., Nakajima, M., Arai, F., Shimizu, T., Kamiya, S. & Fukuda, T. (2007) 'Development of Novel Nanopipette with a Lipid Nanotube as Nanochannel' [2013-09-04]

Piston, D. W. (1998) 'Choosing objective lenses: The importance of numerical aperture and magnification in digital optical microscopy' [2013-09-27]

Schermelleh, L., Heintzmann, R.. & Leonhardt, H. (2010) 'A guide to super-resolution fluorescence microscopy' [2013-05-10]

Sigma-aldrich (2013) *Tutorial Lithography Nanopatterning.* Available from: <http://www.sigmaaldrich.com/materials-science/micro-and-nanoelectronics/lithography-nanopatterning/tutorial.html> [2013-10-10]

Spanner, K. & Vorndran, S. (2003) 'Advances in Piezo-NanoPositioning Technology' [2013-09-27]

Spring, K. R. (2003) 'Fluorescence Microscopy' in *Encyclopedia of Optical Engineering* Marcel Dekker, Inc., New York, pp. 548 - 555

Stepanyants, N. (2013) 'Lipid Nanotubes as a Model for Highly Curved Cellular Membrane Structures' [2013-06-03]

Stepanyants, N., Jeffries, G. D. M., Orwar, O. & Jesorka, A. (2012) 'Radial Sizing of Lipid Nanotubes Using Membrane Displacement Analysis' [2013-06-03]

Stepanyants, N., Näreoja, T., Jesorka, A. & Jeffries, G. M. (2013) ’Studying compositional and environmental effects on the bending rigidity of vesicles and cell plasma membranes using lipid nanotubes’ [2013-06-03]

Sun, Y. & Periasamy, A. (2013) ‘Fluorescence Microscopy Imaging in Biomedical Sciences’ in *Biomedical Optical Imaging Technologies, Biological and Medical Physics, Biomedical Engineering*, ed Liang, R., Springer - Verlag Berlin Heidelberg, pp. 79 - 110

Quercioli, F. (2011) ‘Fundamentals of Optical Microscopy’ in Optical Fluorescence Microscopy, ed A. Diaspro, Springer - Verlag Berlin Heidelberg, pp. 1 - 36

Appendix A - Recipe for photo-litography

Process Step MC2	Tool #	Machine	People (tool responsible)	Process Details
1	628	Megasonic bath and Solvent work	U. Södervall	Clean glass cover slips, H20 is enough with prog. 1 (Power = 100 W, 600s)
2	419	Plasma etch - Plasma Therm BatchTop PE/RIE m/95	G. Alestig	Prog: ash_30s (50 W, 250 mT, 10 sccm) oxygen 250 mTorr
3	400	Sputter - FHR MS150	H. Frederiksen	Al 1kW 60s (1.95 - 2.2 nm/s) --> thickness = 120 nm
4	219	Spinner and low temperature hotplates	B. Nilsson	Spin positive photoresist S1813 (4000 rpm, 30s, 2000ms) and soft bake for 110 © for 90 s
5	213	Mask aligner - KS MA/BA 6	J. Andersson	Align mask
6	213	Mask aligner - KS MA/BA 6	J. Andersson	Exposure 16s (16 s * 6 mW/cm^2 = energi/cm^2)
7	208	Developer baths/wet proc benches	J. Andersson, G. Petersson	Develop resist with base: MF-319 (can use other bench aswell)
8	419	Plasma etch - Plasma Therm BatchTop PE/RIE m/95	G. Alestig	ash_30s Descum
9	623	Hot bath & Acid work	U. Södervall	Etching with Aluminum etchant phosphoric acid:nitric acid:acetic acid:diw (16:1:1:2)
10	624	Liftoff & Solvent work	B. Nilsson	Remove photoresist with 1165 remover, Isopropyl alcohol and water bath with QDR

Appendix B - LabVIEW program for SIM calculation

The frontpanel of the program

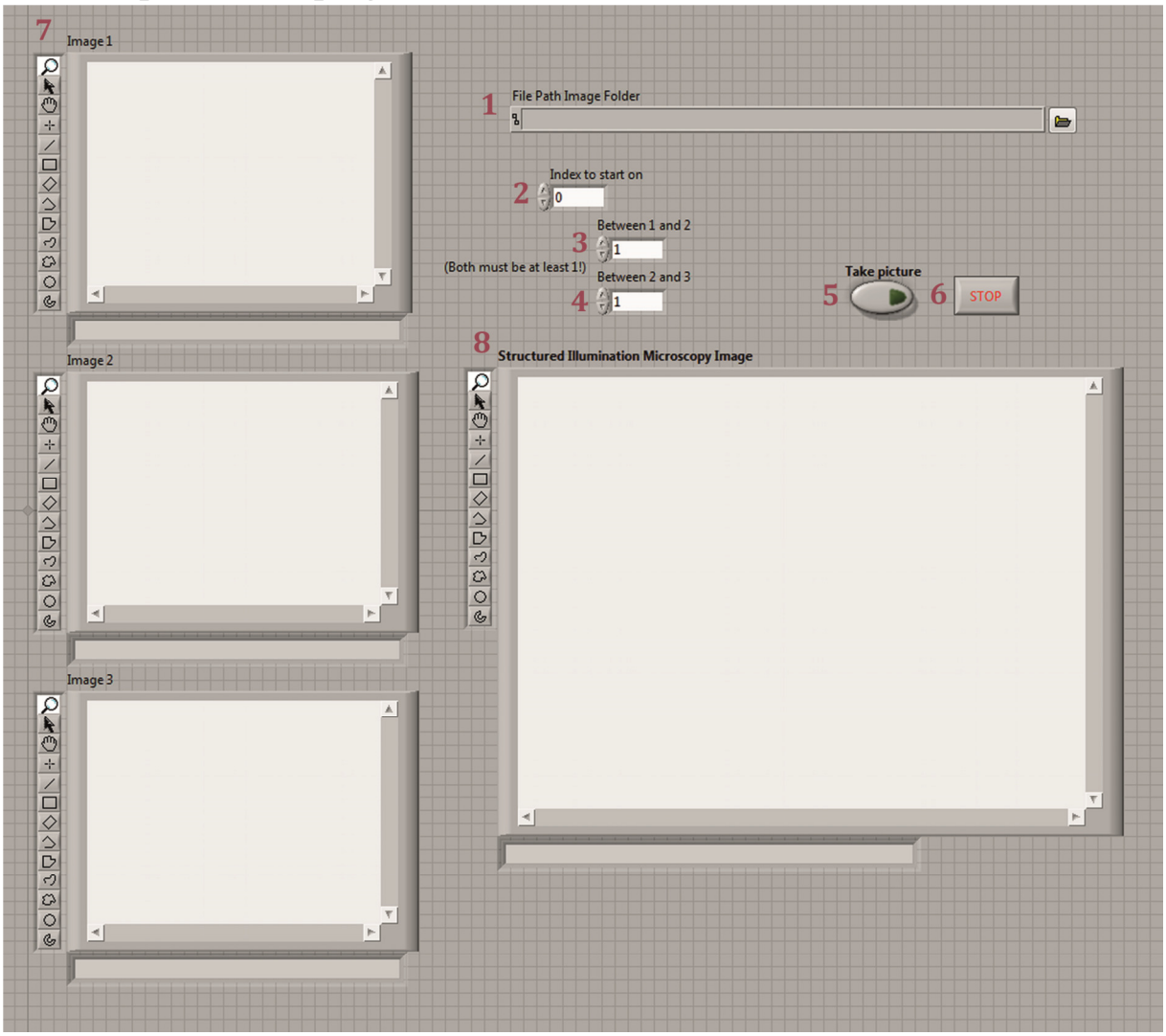

1) File path.
   Selection of the folder containing the image stack to be evaluated. Do check if a sub folder named SIM is present! If so, rename or remove this folder before running the program, else there will be an error message and the program will not run!
2) Index to start on.
   The image stack is read in as an array of image numbers where 0 is the number of the first image in the sequence.
3) Between 1 and 2.
   Default this value is set to 1, which means to read in the next image in the sequence. If it is desired to evaluate how other selections affects the SIM modulations, a higher value, *i.e.* an image later in the sequence, can be chosen. Do not choose 0; this will be the same as the input image 1.

4) Between 2 and 3.
   Same as for *Between 1 and 2* but now between the two last input images. So again, default value is 1 and does not chose 0 since this will be the same as the input image 2.
5) Take picture.
   The output SIM modulated image will be saved in a sub folder named SIM when pressed as this button.
6) Stop.
   Stops the program in a proper way. Avoid stop the program with the stop button in the upper menu bar in LabVIEW.
7) Input images 1, 2 and 3.
   Here, the three chosen input images will be shown.
8) Output image (Structured Illumination Microscopy modulated image)
   Here, the output SIM modulated image will be shown.

The block diagram of the program

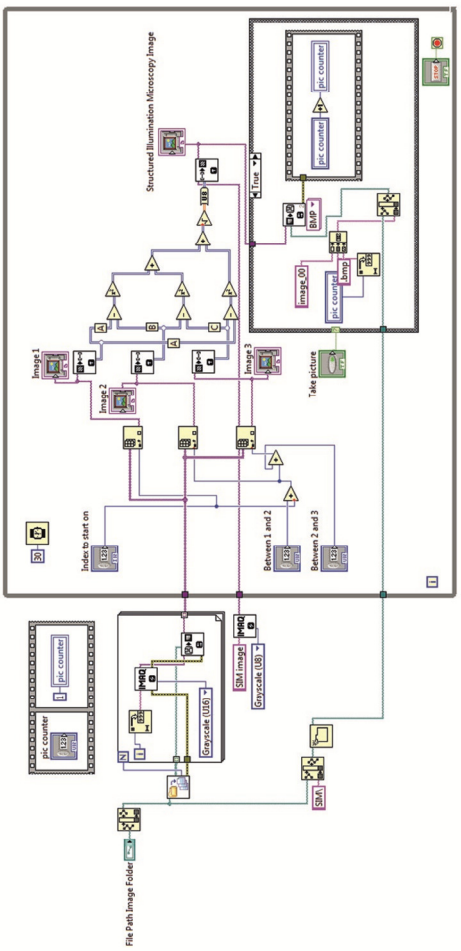

Appendix C - LabVIEW program for Piezo controlling

The frontpanel of the program

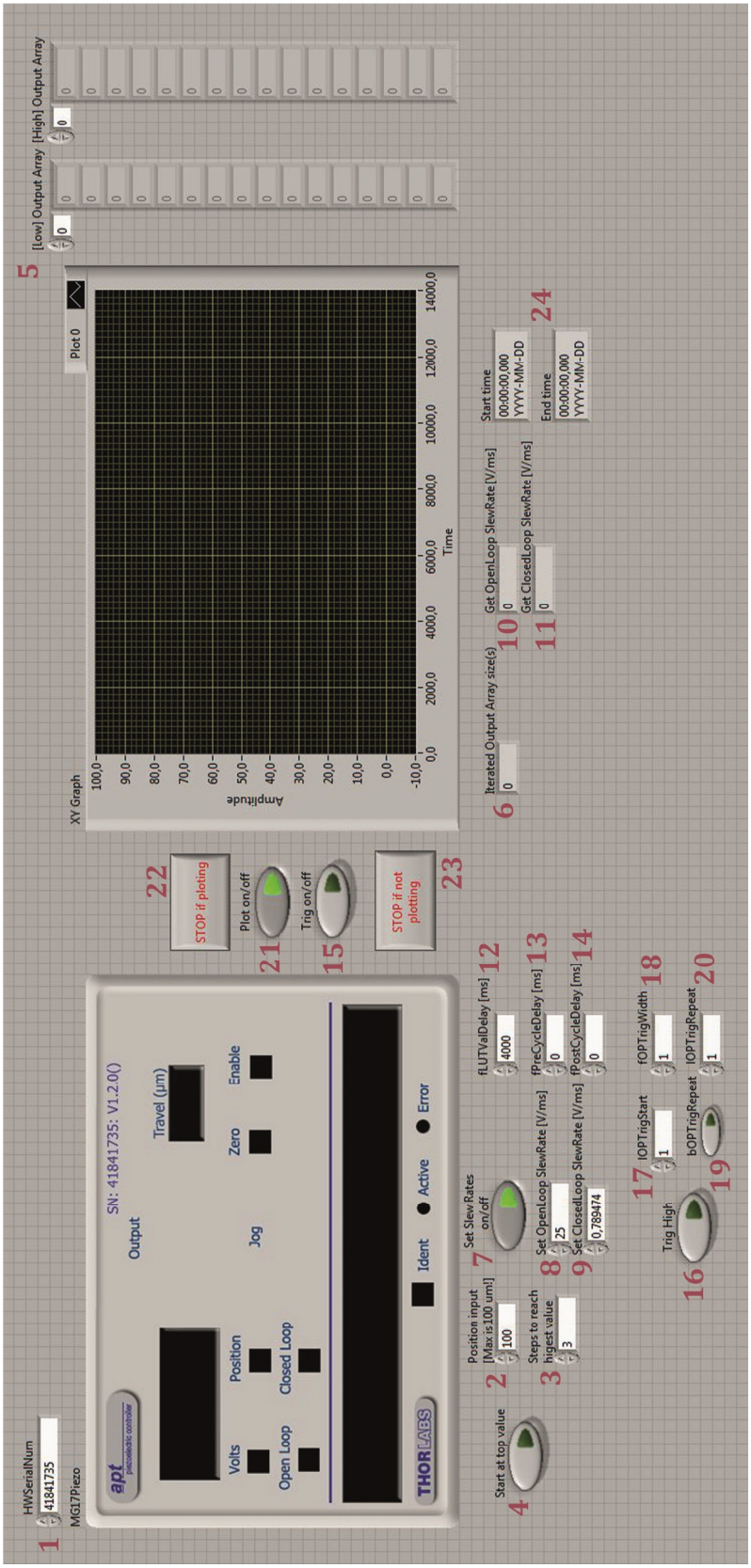

1) HW serial number.
   The correct serial number of the APT must be set in able to run the program. Here is the serial number set to a default value of 41841735 corresponding to the serial number of the APT used.
2) Max travel length.
   The piezo actuator (PAZ015) can operate with a maximum voltage of 75V corresponding to maximum travel length of 100 micrometers. This value is set for the longest distance from 0 in micrometers, *i.e.* the highest step value if several steps are set.
3) Number of steps to reach highest value.
   This value is to set how many steps to take to reach the longest distance from 0. *E.g.* if desired steps are like 0 → 33 → 67 → 100 → 67 → 33 → 0 etc., then set the *Max travel length* = 100 and *Number of steps to reach highest value* = 3.
4) Start at top value.
   If this button is set to on, then the array starting at the highest value instead of at 0, *e.g.* 100 → 67 → 33 → 0→ 33 → 67 → 100 etc.
5) Output array.
   Here, the iterated array is seen as either *[Low]* or as *[High] Output Array* depending whether the *Start at top value* button is set to off or on.
6) Output array length.
   The length of the *Output array* is shown here.
7) Slew rate on/off.
   In order to set *Slew rate* this button should be set to on and then the desired values for each *Open Loop Slew Rate* and *Closed Loop Slew Rate*.
8) Open Loop Slew Rate.
   The slow rate must be at maximum 25 V/ms for open loop operations and this value is also set as a default value.
9) Closed Loop Slew Rate.
   Slew rate for closed loop operations is even slower than for the open loop, but no recommendations are given for this value.
10) Open loop.
    Here, the actual value for slew rate in open loop is read.
11) Closed loop.
    Here, the actual value for slew rate in closed loop is read.
12) fLUTvalDelay.
    According to the method description for SetOutputLUTParams in APT Server Help, this delay value is to set a delay time in milliseconds that the system waits after it sets each array output value. But in reality it is more a value for how long the delay time for the entire array rather than between the values.
13) fpreCycleDelay.
    This delay value is to set a delay time in milliseconds that the system waits before clocking out the array values.

14) fpostCycleDelay.
    This delay value is to set a delay time in milliseconds after the system has sent out the array values before repeating the cycle.
15) Trig on/off.
    In order to set triggering out this button should be set to on and then the desired values for each *Trig High*, *IOPTrigStart*, *fOPTrigWidth*, *bOPTrigRepeat*, *IOPTrigRepeat*.'
16) Trig high.
    If the trigger outputs should go from low to high, i.e. on the rising slope, then this button should be set to on. Elsewise, the trigger outputs will go from high to low, i.e. on the falling slope.

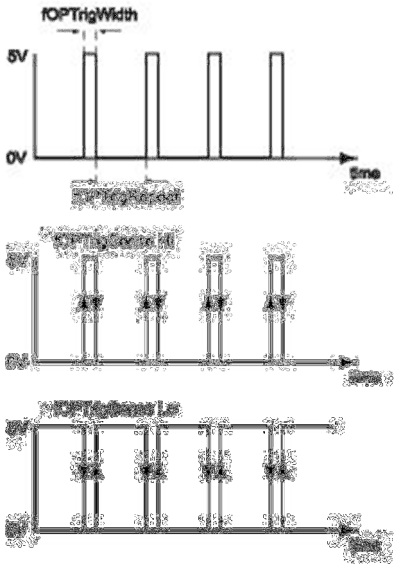

Figure 1 An illustration of the lenghts TrigWidth and TrigRepeat, and also the differences between when triggering from low to high or from high to low (from APT Server Help, Thorlabs).

17) Trig start.
    According to the method description GetOutputLUTTrigParams in APT Server Help, this value specifies at what position in the array where to initiate the output trigger. Attention: It seems not to work when choosing the first position in the array.
18) Trig width.
    This value is to set the width of the output triggers in milliseconds.
19) Trig repeat on.
    In order to repeat the triggering this button should be set to on.
20) Trig repeat.
    This value specifies how often the triggering should be performed within the array, *e.g.* if there should be a trigger output sent for every second value in the array.
21) Plot on.
    In order to plot the positions while running this button should be set to on. This is a slow method and needs long delays in order to show a fairly correct plot, due to sending get commands for reading out values over a USB connection.
22) Stop if plotting.
    A stop button to end the program in a proper way when plotting is set to on.

Attention: If you stop the program with the stop button in the upper menu bar in LabVIEW the controller will not get a stop command for the array looping and the APT will continue looping the array even if the program is no longer running!

23) Stop if not plotting.
    A stop button to end the program in a proper way when plotting is set to off. This extra stop button exists due to that this function is within another while loop.
    Attention; If you stop the program with the stop button in the upper menu bar in LabVIEW the controller will not get a stop command for the array looping and the APT will continue looping the array even if the program is no longer running!
24) Start time.
    This time stamp is from when the array is sent out to the APT.
25) End time.
    This time stamp is from when the program is stopped.

The block diagram of the program